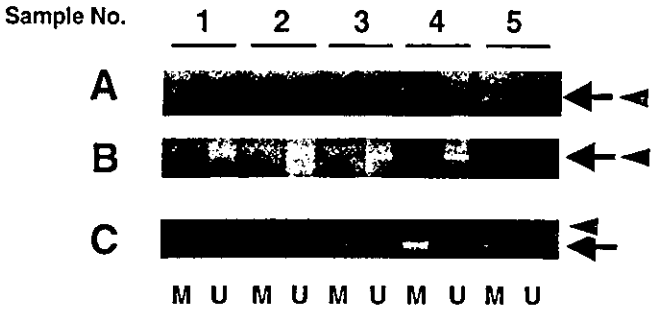

Fig. 2. MSPCR analysis of the CpG island and 5′-noncoding region of the *SOCS-1* from 22 HCC tissue samples. With the same primers used in Fig. 1, 22 pairs of HCC and non-HCC samples were analyzed by MSPCR. Representative cases are shown. Samples *1* and *2* were well-differentiated HCC, *3* and *4* were moderately differentiated HCC, and *5* was poorly differentiated HCC. Panel **B** shows their non-HCC counterparts. **A** MSPCR of DNA from HCC tissue samples with the primers in CpG island. **B** MSPCR of DNA from non-HCC tissue samples with the primers in CpG island. **C** MSPCR of DNA from HCC tissue samples with the primers in 5′-noncoding region. The *arrow* indicates the position of the methylation-specific band; the *arrowhead* indicates the position of the unmethylation-specific band HCC, hepatocellular carcinoma; M, MSPCR with methylation-specific primers; U, MSPCR with unmethylation-specific primers

and an unmethylation-specific band, respectively, when the primers in the CpG island were used. In 9 HCC tissue samples the band indicative of aberrant methylation in the CpG island was detected, while the band indicating unmethylation was detected in 1 HCC tissue sample (Fig. 2). In contrast, in the corresponding non-HCC tissue samples, only 1 exhibited the methylation pattern, whereas the unmethylation pattern was observed in 5 non-HCC tissue samples. Thus, aberrant methylation of *SOCS-1* was significantly associated with HCC rather than with non-HCC tissues ($P = 0.0076$ by Fisher's exact test).

Using primers in the 5′-noncoding promoter region, 14 and 15 HCC tissue samples were informative for a methylation-specific band and an unmethylation-specific band, respectively. Aberrant methylation was observed in 12 HCC tissue samples whereas the unmethylation pattern was detected in 5 HCC tissue samples. In contrast, only 2 non-HCC tissues exhibited aberrant methylation whereas the unmethylation pattern was detected in 10 non-HCC tissues: there was also a significant correlation between HCC and aberrant methylation of *SOCS-1* ($P = 0.0042$).

Neither a methylation-specific nor an unmethylation-specific band in 12 HCC and 16 non-HCC tissues was detected using the primers in the CpG island and in 5 HCC and 10 non-HCC tissue samples using the primers in the 5′-noncoding promoter region, suggesting that *SOCS-1* in these tissues was in a mosaic state of methylation. This suggestion was examined using a hepatoma cell line HLF: neither a methylation- nor an unmethylation-specific band was detected, but after 5-azacytidine treatment of the cell line for 3 days, which cancels methylation of the gene,[22] an unmethylation-specific band appeared, demonstrating that *SOCS-1* in the cell line is methylated in a mosaic fashion. Consequently, *SOCS-1* gene expression was turned on as determined by RT-PCR.

Correlation between SOCS-1 methylation and clinicopathological findings

The relationship between the methylation status of *SOCS-1* and clinicopathological findings is shown in Table 1. When the methylation status in HCC tissue samples was correlated with parameters such as the presence or absence of cirrhosis as the underlying liver disease, the histological degree of HCC, tumor sizes, vascular invasion, distant metastasis, or tumor stages, no significant association was noted.

Discussion

In the current study, we analyzed the methylation status of *SOCS-1*, a negative regulator of the JAK/STAT pathway, by the MSPCR method. Using the primers located in the CpG island in the coding region, aberrant methylation was observed in 9 of 22 (41%) HCC tissue samples, and 12 of 22 (54.5%) HCC tissue samples by the use of primers in the 5′-noncoding region. The former rate is almost compatible with the incidence in a previous report.[14] It is notable that a similar or higher rate of aberrant methylation was detected in the 5′-noncoding promoter region of *SOCS-1*. It is established that methylation in the promoter region is essential in the regulation of (silencing) the genes.[16,17] The frequent occurrence of aberrant methylation in the promoter region of *SOCS-1* further supports the notion that the downregulation of SOCS-1 expression is common in human HCC. Very recently, methylation in the promoter of SOCS-1 gene was reported in pancreatic tumors.[23]

In our MSPCR analysis, a substantial number of samples showed neither the methylated nor unmethylated pattern. The reason for this dual negativity is unclear. One possibility is a mosaic methylation pattern that may exist in the *SOCS-1*. If not all the susceptible cytosine residues are methylation, i.e., a gene is methylated in a mosaic fashion, one cannot determine the methylation status by MSPCR. This possibility was confirmed using a hepatoma cell line, as shown in the Results section. Neither a methylation- nor an unmethylation-specific band was detected, but after

5-azacytidine treatment of the cell line for 3 days, which cancels methylation of the gene,[22] an unmethylation-specific band appeared, demonstrating that *SOCS-1* in the cell line is methylated in a mosaic fashion.

SOCS-1 transcription is activated by signal transducer and activator of transcription (STAT) and the resultant proteins negatively regulate the JAK/STAT pathways either by directly inhibiting JAKs or by binding to receptors and blocking further association with STATs. Of the eight SOCS family members, SOCS-1 is a negative regulator of IL-6 signals. The silencing of *SOCS-1* results in constitutive activation of the JAK/STAT pathway. Without negative feedback by SOCS-1, the downstream pathways and target genes are strongly activated.[24] There are several lines of evidence supporting the idea that the JAK/STAT pathway may be involved in oncogenesis. The constitutive activation of the JAK/STAT pathway including STAT3 is observed in a number of transformed cells.[25] Thus, SOCS-1 is considered to be a tumor suppressor candidate, which chiefly has a role in the development of hematopoietic malignancies.[26] Also, an association of the SOCS-1 in hepatocarcinogenesis has recently been suggested.[15] There are a variety of gene products in the downstream of the JAK/STAT pathway, including c-*myc* or c-*fos*.[27] The activation of the pathway thus may cause an activation of oncogenes or growth-associated genes and eventually lead to oncogenesis. The precise role of SOCS-1 in hepatocarcinogenesis is currently unclarified and requires further study, but it might play an essential role in the majority of HCCs.

Our current results confirmed those of a previous study[14] and added a new piece of information on methylation of the promoter region of *SOCS-1*. However, the presence of cases negative for both methylation and unmethylation may limit the application of this technique for the analysis of hepatocarcinogenesis. In addition, recently the association between the core protein of hepatitis C virus and the JAK/STAT pathway has been reported as a potential proliferator of hepatocytes.[28] Besides aberrant methylation, association of SOCS-1 with HCV may cause a down-regulation of *SOCS-1* expression. In relation to this issue, it is interesting to note that a few patients in our series exhibited aberrant methylation of *SOCS-1* in the adjacent non-HCC tissue samples. Infection with HCV, which is present in all patients, may be associated with *SOCS-1* expression in human HCC tissues. Further studies are necessary for deciphering the complicated involvement of the SOCS-1 and JAK/STAT pathway in hepatocarcinogenesis, possibly in association with HCV infection.

References

1. Chen CJ, Yu MW, Liaw YF. Epidemiological characteristics and risk factors of hepatocellular carcinoma. J Gastroenterol Hepatol 1997;12:S294–308.
2. Saito I, Miyamura T, Ohbayashi A, Harada H, Katayama T, Kikuchi S, et al. Hepatitis C virus infection is associated with the development of hepatocellular carcinoma. Proc Natl Acad Sci U S A 1990;87:6547–9.
3. Robinson WS. Molecular events in the pathogenesis of hepadnavirus-associated hepatocellular carcinoma. Annu Rev Med 1994;45:297–323.
4. Umeda T, Hino O. Molecular aspects of human hepatocarcinogenesis mediated by inflammation: from hypercarcinogenic state to normo- or hypocarcinogenic state. Oncology 2002;62:38–42.
5. Kim CM, Koike K, Saito I, Miyamura T, Jay G. HBx gene of hepatitis B virus induces liver cancer in transgenic mice. Nature (Lond) 1991;351:317–20.
6. Moriya K, Fujie H, Shintani Y, Yotsuyanagi H, Tsutsumi T, Matsuura Y, et al. The core protein of hepatitis C virus induces hepatocellular carcinoma in transgenic mice. Nat Med 1998; 41065–7.
7. Lerat H, Honda M, Beard MR, Loesch K, Sun J, Yang Y, et al. Steatosis and liver cancer in transgenic mice expressing the structural and nonstructural proteins of hepatitis C virus. Gastroenterology 2002;122:352–65.
8. Koike K, Tsutsumi T, Fujie H, Shintani Y, Moriya K. Role of hepatitis viruses in hepatocarcinogenesis. Oncology 2002;62:29–37.
9. Satoh S, Daigo Y, Furukawa Y, Kato T, Miwa N, Nishiwaki T, et al. AXIN1 mutations in hepatocellular carcinomas, and growth suppression in cancer cells by virus-mediated transfer of AXIN1. Nat Genet 2000;24:245–50.
10. Fujie H, Moriya K, Shintani Y, Tsutsumi T, Takayama T, Makuuchi M, et al. Frequent β-catenin aberration in human hepatocellular carcinoma. Hepatol Res 2001;20:39–51.
11. Matsuda Y, Ichida T, Matsuzawa J, Sugimura K, Asakura H. p16(INK4) is inactivated by extensive CpG methylation in human hepatocellular carcinoma. Gastroenterology 1999;116:394–400.
12. Starr R, Willson TA, Viney EM, Murray LJ, Rayner JR, Jenkins BJ, et al. A family of cytokine-inducible inhibitors of signaling. Nature (Lond) 1997;387:917–21.
13. Endo TA, Masuhara M, Yokouchi M, Suzuki R, Sakamoto H, Mitsui K, et al. A new protein containing an SH2 domain that inhibits JAK kinases. Nature 1997;387:921–4.
14. Naka T, Matsumoto T, Narazaki M, Fujimoto M, Morita Y, Ohsawa Y, et al. Accelerated apoptosis of lymphocytes by augmented induction of Bax in SSI-1 (STAT-induced STAT inhibitor-1) deficient mice. Proc Natl Acad Sci U S A 1998;95: 15577–82.
15. Yoshikawa H, Matsubara K, Qian GS, Jackson P, Groopman JD, Manning JE, et al. SOCS-1, a negative regulator of the JAK/STAT pathway, is silenced by methylation in human hepatocellular carcinoma and shows growth-suppression activity. Nat Genet 2001;28:29–35.
16. Jaenisch R, Bird A. Epigenetic regulation of gene expression: how the genome integrates intrinsic and environmental signals. Nat Genet 2003;33:245–54.
17. Herman JG, Baylin SB. Promoter-region hypermethylation and gene silencing in human cancer. Curr Top Microbiol Immunol 2000;249:35–54.
18. Desmet VJ, Gerber M, Hoofnagle JH, Manns M, Scheuer PJ. Classification of chronic hepatitis: diagnosis, grading and staging. Hepatology 1994;19:1513–20.
19. Hermanek P, Sobin LH. UICC TNM classification of malignant tumors. 4th ed. Berlin: Splinger; 1987.
20. Yotsuyanagi H, Yasuda K, Iino S, Moriya K, Fujie H, Shintani Y, et al. Persistent viremia after recovery from self-limited acute hepatitis B. Hepatology 1998;27:1377–82.

21. Herman JG, Graff JR, Myohanen S, Nelkin BD, Baylin SB. Methylation-specific PCR: a novel PCR assay for methylation status of CpG islands. Proc Natl Acad Sci U S A 1996;93:9821–6.
22. Velicescu M, Weisenberger DJ, Gonzales FA, Tsai YC, Nguyen CT, Jones PA. Cell division is required for de novo methylation of CpG islands in bladder cancer cells. Cancer Res 2002;62:2378–84.
23. House MG, Guo M, Iacobuzio-Donahue C, Herman JG. Molecular progression of promoter methylation in intraductal papillary mucinous neoplasms (IPMN) of the pancreas. Carcinogenesis (Oxf) 2003;24:193–8.
24. Greenhalgh CJ, Miller ME, Hilton DJ, Lund PK. Suppressors of cytokine signaling: relevance to gastrointestinal function and disease. Gastroenterology 2002;123:2064–81.
25. Kishimoto T, Kikutani H. Knocking the SOCS off a tumor suppressor. Nat Genet 2001;28:4–5.
26. Rottapel R, Ilangumaran S, Neale C, La Rose J, Ho JM, Nguyen MH, et al. The tumor suppressor activity of SOCS-1. Oncogene 2002;21:4351–62.
27. Darnell JE Jr, Kerr IM, Stark GR. Jak-STAT pathways and transcriptional activation in response to IFNs and other extracellular signaling proteins. Science 1994;264:1415–21.
28. Yoshida T, Hanada T, Tokuhisa T, Kosai K, Sata M, Kohara M, et al. Activation of STAT3 by the hepatitis C virus core protein leads to cellular transformation. J Exp Med 2002;196:641–53.

ELSEVIER

Journal of Hepatology 42 (2005) 110–116

Journal of Hepatology

www.elsevier.com/locate/jhep

Involvement of mitochondrial permeability transition in acetaminophen-induced liver injury in mice

Yasuhiro Masubuchi, Chieko Suda, Toshiharu Horie*

Department of Biopharmaceutics, Graduate School of Pharmaceutical Sciences, Chiba University, 1-8-1 Inohana, Chuo-ku, Chiba 260-8675, Japan

***Background/Aims*: Although mitochondria have been demonstrated as primary targets in acetaminophen hepatotoxicity, the mechanism for mitochondria-mediated toxicity has not been defined. We examined the role of mitochondrial permeability transition (MPT) in the acetaminophen-induced liver injury.**

***Methods*: Male CD-1 mice were given intraperitoneally acetaminophen (350 mg/kg) without or with cyclosporin A (50 mg/kg), a specific inhibitor of MPT. Serum alanine aminotransferase (ALT), a marker of liver injury, and other biochemical parameters were determined.**

***Results*: Acetaminophen-induced ALT leakage was attenuated by co-administration of cyclosporin A. Cyclosporin A did not affect acetaminophen-induced early decrease in hepatic reduced glutathione (GSH) contents, indicating lack of the effect on the metabolic activation. Acetaminophen-induced decrease in mitochondrial GSH and ATP contents, and cytosolic leakage of cytochrome c were attenuated by cyclosporin A, suggesting that mitochondrial oxidative stress and ATP depletion resulting from MPT are principle mechanisms involved in acetaminophen-induced liver injury. Mitochondrial swelling by calcium was exacerbated in the mitochondria isolated from the acetaminophen-treated mice. In vitro exposure of intact mitochondria to *N*-acetyl-*p*-benzoquinone imine (NAPQI) with calcium caused mitochondrial swelling.**

***Conclusions*: The present data indicate that the MPT is the principal mechanism in the acetaminophen-induced liver injury and NAPQI is a candidate to open the transition pore.**

***Keywords*: Acetaminophen; Liver injury; Mitochondrial permeability transition; Cyclosporin A; Glutathione; ATP; Cytochrome c; *N*-Acetyl-*p*-benzoquinone imine**

1. Introduction

An overdose of the analgesic drug acetaminophen causes liver injury in experimental animals and humans. The toxicity has been shown to be initiated by cytochrome P450 metabolism to *N*-acetyl-*p*-benzoquinone imine (NAPQI) [1,2]. The high reactivity of NAPQI with sulfhydryl groups results in depleting glutathione in hepatocytes, followed by covalent binding to intracellular proteins [3,4]. Although it has been shown that the relative amount of covalent binding is correlated with the development of the toxicity [3], it is also suggested that the covalent binding is not sufficient for the toxicity [5–7]. Extensive studies were thus focused on covalent binding to specific protein(s) as a trigger of the toxicity. A number of proteins have been identified as targets of NAPQI by the immunological techniques [8] and recent proteomics [9]. Because development of various mitochondria dysfunctions has been observed with acetaminophen toxicity, which include inhibition of respiration, a decrease in hepatic ATP levels, a decrease in membrane potential, a loss of mitochondrial Ca^{2+} [10–13], it was proposed that mitochondria was primary target of the reactive metabolite. Indeed, some of the target proteins were localized in mitochondria fraction including glutamate dehydrogenase, aldehyde dehydrogenase, carbamyl phosphate synthetase-I and ATP synthetase α-subunit [8,9]. These enzyme activities in the mitochondrial fraction were decreased partially [14,15], probably as consequences of covalent binding, while it is

Received 27 April 2004; received in revised form 16 September 2004; accepted 21 September 2004; available online 12 October 2004

* Corresponding author. Tel./fax: +81 43 226 2886.
E-mail address: horieto@p.chiba-u.ac.jp (T. Horie).

0168-8278/$30.00
doi:10.1016/j.jhep.2004.09.015

also estimated that only the loss of the any single enzyme activity could not explain mitochondria-mediated acetaminophen hepatotoxicity. It is thus presumed that the toxicity is accounted for by combination of covalent binding to several functional proteins and/or by secondary event following the covalent binding.

Mitochondrial permeability transition (MPT) is recently focused as a mechanism for drug-induced hepatocyte injury [16–18]. The MPT represents an abrupt increase in permeability of the mitochondrial inner membrane to allow solutes with a molecular weight less than 1500 [19]. The MPT is promoted by the accumulation of excessive Ca^{2+} and stimulated by various compounds and conditions. It leads to dissipation of membrane potential ($\Delta\psi$), uncoupling of oxidative phosphorylation, loss of pre-accumulated Ca^{2+}, and expansion of the matrix volume. MPT causes both apoptotic and necrotic cell death. Acetaminophen could induce hepatocyte apoptosis in vitro as well as necrosis [16,17], whereas the quantitative determination of cell death after exposure of hepatotoxic dose of acetaminophen in vivo indicated that acetaminophen caused extensively oncotic necrosis rather than apoptosis [20]. Recent papers proposed the possibility of MPT as a mechanism for acetaminophen-induced liver injury [21,22], but have not been fully supported by experimental data. In the present study, we investigated the possible involvement of MPT in acetaminophen-induced liver injury in male CD-1 mice by using a MPT specific inhibitor, cyclosporin A.

2. Materials and methods

2.1. Chemicals

Acetaminophen and NAPQI were purchased from Sigma-Aldrich (St Louis, MO); cyclosporin A, glutathione, reduced form (GSH) and glutathione disulfide (GSSG) were from the Wako Pure Chemical Ind. (Osaka, Japan); ATP was from Oriental Yeast Co., Ltd (Tokyo, Japan). All other chemicals and solvents were of analytical grade.

2.2. Animals and in vivo treatment

Male CD-1 mice were purchased from Takasugi Experimental Animals (Saitama, Japan). The mice were used in the experiment at the age of 8–9 weeks. The mice were acclimatized at least 1 week in a climate-controlled room on a 12-hour light-dark cycle and were fed ad libitum. All procedures and care were carried out according to the National Institutes of Health Guide for the Care and Use of Laboratory animals. The mice were then fasted for 16 h before experiments to sensitize mice to acetaminophen toxicity by decreasing basal levels of liver GSH. Mice received intraperitoneally (i.p.) 10-ml/kg saline or 350 mg/kg of acetaminophen. In some experiments, mice received 10-ml/kg i.p. corn oil or cyclosporin A (50 mg/kg) in the oil just before saline or acetaminophen. Two, 8 or 24 h after the treatment, blood of the mice was collected and the mice were killed to obtain their livers. A portion of the liver was fixed in 10% buffered formalin for histological sections. The blood was allowed to coagulate and the samples were then centrifuged to obtain the serum. In some experiments, the bile duct was cannulated with polyethylene tubing (PE 10) to allow sampling of bile and the bile was collected for 15 min.

2.3. Assessment of hepatotoxicity

Serum alanine aminotransferase (ALT) activities were assayed as a marker of acetaminophen-induced hepatotoxicity. Assays were run on the test kit (Sigma Diagnostics, St Louis, MO). Formalin-fixed tissue sections were embedded in paraffin, mounted onto glass slides, and stained with hematoxylin–eosin (Takasaki Pathologic Center, Gunma, Japan). Hepatotoxicity was also assessed by histological examination of the tissue sections.

2.4. Isolation of liver mitochondria

Liver mitochondrial fraction was prepared according to the method described by Schneider and Hogeboom [23] with modifications. The livers were isolated and placed in the ice-cold medium containing 250 mM sucrose, 10 mM HEPES-KOH, pH 7.4, and 0.5 mM EGTA. The livers were cut to small cubes with scissors in 50 ml of the medium and homogenized five times in a Potter homogenizer. The homogenates were diluted to 100 ml per liver and were centrifuged at 770×*g* for 5 min kept at 4 °C. The resulting supernatant was decanted and further centrifuged at 9800×*g* for 10 min. The supernatant was discarded, the pellet was suspended in 20 ml of the ice-cold isolation medium, and centrifuged at 4500×*g* for 10 min. The final mitochondrial pellet was suspended in 1 ml of medium containing 250 mM sucrose and 10 mM HEPES-KOH, pH 7.4. Protein concentration of the mitochondrial fraction was determined by the method of Lowry et al. [24].

2.5. Assay of GSH and GSSG

GSH and GSSG contents in liver homogenates, mitochondria and bile were determined by an HPLC method according to Keller and Menzel [25] with modifications. The reaction medium (1.0 ml) was mixed with 0.5 ml solution consisting of 5% metaphosphoric acid/0.1% EDTA (2:7, v/v). The sample was centrifuged (16,000×*g*, 5 min) and the supernatant (0.5 ml) mixed with 10 ml of 250 mM 3-fluorotyrosine as an internal standard for HPLC. The samples were applied after filtration to the HPLC column (Inertsil ODS, GL Sciences Inc., Tokyo). The mobile phase consisting of 0.1% trifluoroacetic acid/methanol (9/1, v/v) was pumped at a flow rate of 1.0 ml/min. The effluent from the column was mixed with luminescence reagent consisting of 18.6 mM o-phthalaldehyde and 17.1 mM 2-mercaptoethanol pumped at a flow rate of 0.2 ml/min. The fluorescence intensity at the 355/425 nm wavelength pair was monitored.

2.6. Assay of mitochondrial ATP content

Liver mitochondria were suspended into 0.5 ml of 1N $HClO_4$ and disrupted by vortex mixing with the acid. After the neutralization with 2N KOH, the sample was centrifuged (16,000×*g*, 30 s) and supernatant was used for assay for ATP. ATP content was measured with Sigma ATP bioluminescent assay kit based on the luciferin-luciferase method by a chemiluminescence analyzer.

2.7. Detection of cytochrome c in cytosol

Cytochrome c in hepatic cytosol fraction was detected by immunoblot analysis. Cytosolic proteins (5.0 μg) were separated by SDS–PAGE with a 15% polyacrylamide gel. The proteins on the gel were transferred to a polyvinylidine difluoride membrane (Bio-Rad Laboratories, Hercules, CA, USA). The membrane was treated with the anti-cytochrome c antibody (clone 7H8.2C12, Lab Vision Co., Fremont, CA), which was diluted 1:1000 for use. The immunoblots were developed with the enhanced chemiluminescence detection method with reagents from Amersham Pharmacia Biotech (Uppsala, Sweden), according to the manufacturer's instructions.

2.8. Incubation of mitochondria

Reaction medium containing 1.0 mg/ml liver mitochondrial protein, 125 mM sucrose, 150 mM KCl, 10 mM HEPES-KOH, and 2.5 μM

rotenone was preincubated at 30 °C. The liver mitochondria from acetaminophen-treated or control mice were energized by 5 mM succinate. The incubation was started by adding 20 μM $CaCl_2$ and was performed at 30 °C for various time periods. In the experiment to determine in vitro effects of acetaminophen and NAPQI, the liver mitochondria from untreated mice in the above-mentioned mixture with 20 μM $CaCl_2$ were energized by 5 mM succinate. The incubation was started by adding acetaminophen or NAPQI and was performed at 30 °C for various time periods. In some experiments, the mixture included 1 μM cyclosporin A.

2.9. Assessment of mitochondrial permeability transition

Mitochondrial swelling as the indicator of MPT was estimated from the decrease in absorbance at 540 nm.

2.10. Assessment of mitochondrial membrane potential

The electrical transmembrane potential of mitochondria was monitored spectrophotometrically with the cationic dye, rhodamine 123 at the concentration of 0.5 μM. After the 2-min preincubation with succinate, incubation was started by the addition of acetaminophen or NAPQI and was performed for 3 min. The reaction medium was immediately centrifuged (16,000×*g*, 30 s) and fluorescence intensity of the supernatant was monitored at the 505/535 nm wavelength pair. $\Delta\psi$ was calculated by the Nernst equation as described previously [26].

2.11. Statistical analysis

The experimental groups were compared by analysis of variance, followed by Newman–Keuls multiple comparisons test to determine significant differences between the group means.

3. Results

3.1. Protection of mice from acetaminophen-induced liver injury by cyclosporin A

Administration of acetaminophen (350 mg/kg) to male CD-1 mice induced an increase in serum ALT leakage at 8 and 24 h after the injection (Table 1). No significant increase in ALT was observed 2 h after the treatment (data not shown). The ALT leakage was significantly suppressed by co-administration of cyclosporin A (50 mg/kg, i.p.), a typical inhibitor of MPT pore opening, suggesting that MPT is involved in pathogenesis of the acetaminophen-induced liver injury. Cyclosporin A itself was not hepatotoxic under the present condition. Moreover,

Table 1
Effect of cyclosporin A on acetaminophen-induced liver injury

	$ALT_{8\,h}$ (IU/l)	$ALT_{24\,h}$ (IU/l)
Control	12±1	16±4
Cyclosporin A	17±3	11±3
Acetaminophen	1765±541*	2459±548**
Cyclosporin A+ acetaminophen	396±291#	986±260**#

Mice were given acetaminophen (350 mg/kg, i.p.) together with or without cyclosporin A (50 mg/kg, i.p.), and were killed at 8 or 24 h after the treatment. The results are means±SE of 6–12 mice. *$P<0.05$, **$P<0.01$, Significantly different from corresponding control. #$P<0.05$, Significantly different from 'Acetaminophen' group.

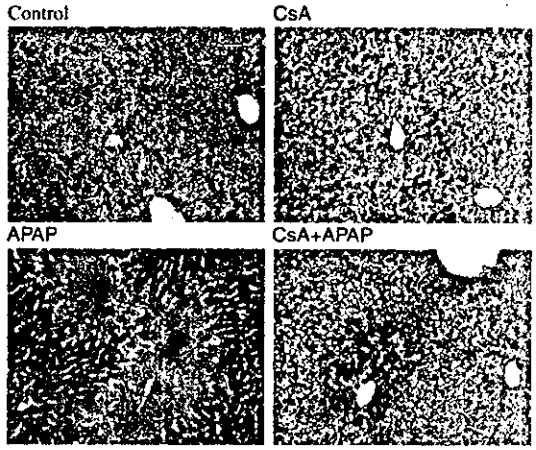

Fig. 1. Histopathology of liver 24 h after administration of acetaminophen. Mice were given acetaminophen (APAP, 350 mg/kg, i.p.) together with or without cyclosporin A (CsA, 50 mg/kg, i.p.), and were killed 24 h after the treatment. Liver sections were subjected to hematoxylin–eosin staining.

histological examination of liver tissues 24 h after treatment with acetaminophen revealed centrilobular necrosis with hemorrhage, whereas the mice treated together with cyclosporin A showed only minimal hepatic necrosis (Fig. 1).

Acetaminophen-induced liver injury is mediated by its reactive metabolite, NAPQI. NAPQI binds to GSH, resulting in depleting hepatic GSH, followed by covalently binding to cellular critical targets. Therefore, an early decrease in hepatic GSH is the reflect of NAPQI formation. The hepatic GSH level markedly decreased 2 h after the acetaminophen treatment, and the decrease was not affected by the coadministration with cyclosporin A (Fig. 2). Similar results were obtained when measured at an earlier time point (30 min; acetaminophen, 2.96±0.71; acetaminophen+ cyclosporin A, 3.24±0.38 nmol/mg protein). The unchanged depletion rate of GSH suggests that the production of NAPQI is not affected by cyclosporin A at

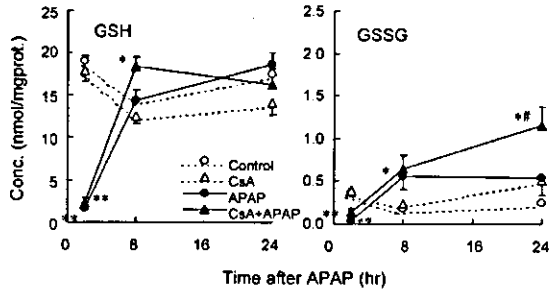

Fig. 2. Time course of hepatic GSH and GSSG contents after administration of acetaminophen. Mice were given acetaminophen (APAP, 350 mg/kg, i.p.) together with or without cyclosporin A (CsA, 50 mg/kg, i.p.), and were killed at various time points. Contents of GSH and GSSG in liver homogenates were determined. The results are means±SE of 3–6 mice. *$P<0.05$, **$P<0.01$, Significantly different from corresponding APAP(−) groups.

least under these experimental conditions. Cyclosporin A is a substrate of CYP3A [27]. While NAPQI formation is mediated mainly by CYP2E1 in mice [28], several reports indicated that other P450 isozymes including CYP3A also contributed to the metabolism [29,30]. Thus, it may be possible for cyclosporin A to inhibit CYP3A-dependent NAPQI generation.

Similar early decrease was also obtained for GSSG (Fig. 2). Because GSH is oxidized to form GSSG, the decrease in GSSG would be associated with the depletion of GSH. The hepatic GSH level was completely recovered 8 h after the injection, whereas hepatic GSSG levels were increased as compared to controls and, furthermore, cyclosporin A potentiated this effect at the later time point (Fig. 2). It is considered that the increases in GSSG is accounted for the oxidative stress secondary to acetaminophen-induced liver injury [21] and by the additional effects of cyclosporin A, which is known to induce oxidative stress [31].

3.2. Changes in mitochondrial parameters in the mice with acetaminophen-induced liver injury

Although, the GSH content in liver homogenate was returned to the control level 8 h after the acetaminophen treatment (Fig. 2), the content in the mitochondria fraction was lower than control at the same time point. Furthermore, mitochondrial GSSG content markedly increased in the treated mice (Fig. 3). These results indicate mitochondrial oxidative stress, which plays an important role in initiation of the acetaminophen hepatotoxicity [32]. The collapse of the mitochondrial redox balance was partially prevented by cyclosporin A (Fig. 3). Similar results were obtained 24 h after the treatment (data not shown). Therefore, increase in tissue GSSG levels observed at 24h after the treatment with cyclosporin A and acetaminophen (Fig. 2) may be derived from outside of mitochondrial compartment. Moreover, biliary excretion of GSSG in this group was higher than other groups (control, 1.85±0.21; cyclosporin A, 2.43±0.46; acetaminophen, 1.97±0.26; cyclosporin A+acetaminophen, 4.67±0.44 nmol/min), whereas that of GSH was unchanged (control, 6.26±0.86; cyclosporin A, 6.42±1.19; acetaminophen, 5.60±0.75; cyclosporin A+acetaminophen, 5.39±1.44 nmol/min). Because GSSG accumulated in the mitochondrial compartment is not released into bile [33], these data support the idea that the increase in liver GSSG at 24 h after the treatment with cyclosporin A and acetaminophen is attributable to the extramitochondrial oxidative stress, which is irrelevant for the liver injury.

Depletion of mitochondrial ATP, which is likely more critical event for the toxicity, was observed in the acetaminophen-treated mice and was also partially prevented in the mice treated with cyclosporin A (Fig. 3). Because mitochondrial oxidative stress and the depletion of ATP has been implicated with MPT [34], the beneficial effects of cyclosporin A support our conclusion that MPT is a key step in the acetaminophen-induced liver injury. Leakage of cytochrome c into cytosol, which is correlated with MPT and a signal for apoptotic cell death, was detected in the acetaminophen-treated mice and was slightly attenuated by the coadministration of cyclosporin A (Fig. 4). This result also demonstrates the opening of the cyclosporin-sensitive MPT pore in the acetaminophen hepatotoxicity. MPT is characterized by a progressive permeabilization of the inner mitochondrial membrane dependent on the excessive amount of intramitochondrial Ca^{2+} and results in mitochondrial swelling [16,17]. Energized mitochondria from control mice tolerated Ca^{2+} at the concentration of 20 μM without undergoing the MPT as assessed by mitochondrial swelling (Fig. 5). By contrast, mitochondria from acetaminophen-treated mice were much more sensitive to the MPT induction. A large-amplitude swelling was observed with mitochondria from the treated mice and was prevented by the addition of cyclosporin A (1 μM) into the reaction medium (Fig. 5).

3.3. In vitro effects of acetaminophen and NAPQI on isolated mitochondria

Incubation of energized mitochondria in the presence of Ca^{2+} (20 μM) and NAPQI (5–50 μM) induced a large-

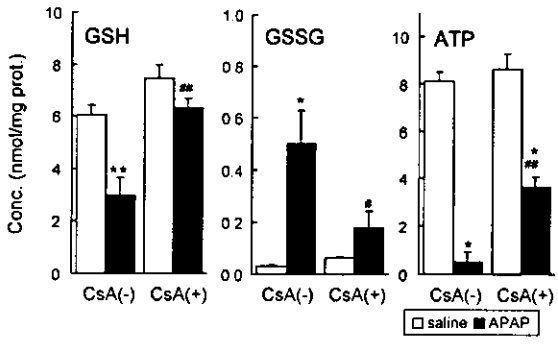

Fig. 3. Mitochondrial GSH, GSSG and ATP contents after administration of acetaminophen. Mice were given acetaminophen (APAP, 350 mg/kg, i.p.) together with or without cyclosporin A (CsA, 50 mg/kg, i.p.), and were killed 8 h after the treatment. Contents of GSH, GSSG and ATP in liver mitochondria were determined. The results are means±SE of 3–6 mice. *$P<0.05$, **$P<0.01$, Significantly different from corresponding APAP(−) groups. #$P<0.05$, ##$P<0.01$, Significantly different from corresponding CsA(−) groups.

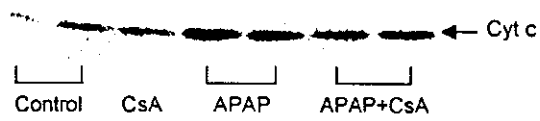

Fig. 4. Leakage of cytochrome c to cytosol after administration of acetaminophen. Mice were given acetaminophen (350 mg/kg, i.p.) together with or without cyclosporin A (50 mg/kg, i.p.), and were killed 24 h after the treatment. Hepatic cytosol fractions from the mice were analyzed by Western blot analysis with antibody against cytochrome c. Each lane represents a sample from a single mouse. The results are representative blots from 3 to 5 mice.

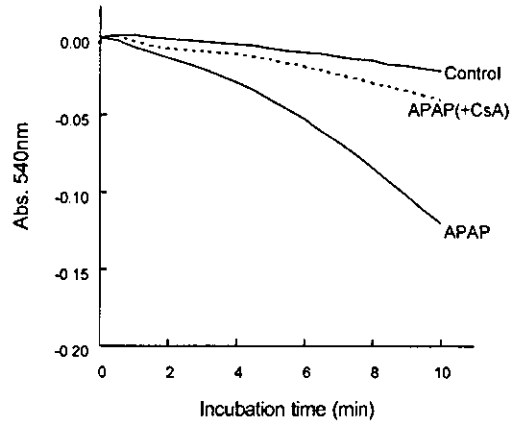

Fig. 5. Swelling of liver mitochondria from mice after administration of acetaminophen. Mice were given acetaminophen (350 mg/kg, i.p.) and were killed 8 h after the treatment along with control mice. Mitochondria (1 mg/ml) of the mice were incubated in the reaction medium containing 125 mM sucrose, 150 mM KCl, 10 mM HEPES-KOH, 2.5 μM rotenone, 20 μM $CaCl_2$, and was energized by 5 mM succinate. Absorbance at 540 nm was monitored after adding $CaCl_2$. The dotted line shows the incubation of mitochondria from acetaminophen-treated mice with 1 μM cyclosporin A. The results are representatives from 3 to 5 experiments.

amplitude swelling (Fig. 6). Addition of cyclosporin A (1 μM) prevented the mitochondrial swelling induced by NAPQI. On the other hand, acetaminophen did not induce swelling at the acetaminophen concentration up to 5 mM

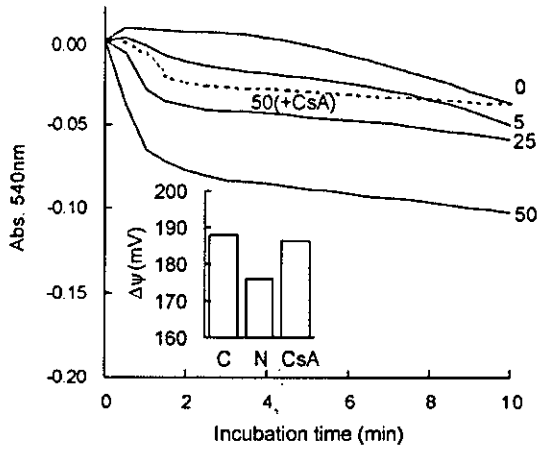

Fig. 6. Swelling and depolarization of liver mitochondria from mice in vitro treated with NAPQI. Mitochondria (1 mg/ml) of untreated mice were incubated in the reaction medium containing 125 mM sucrose, 150 mM KCl, 10 mM HEPES-KOH, 2.5 μM rotenone, 20 μM $CaCl_2$, 5–50 μM NAPQI and were energized by 5 mM succinate. Absorbance at 540 nm was monitored after adding NAPQI. Numbers in the figure are concentrations (μM) of NAPQI. The dotted line shows the incubation of mitochondria with 50 μM NAPQI and 1 μM cyclosporin A. The plots inserted are $\Delta\psi$ values obtained from the fluorescence intensity at the 505/535 nm wavelength pair after incubation of the same mixture with 0.5 mM rhodamine 123. The addition of chemicals (C, no addition; N, 50 μM NAPQI; CsA, 50 μM NAPQI + 1 μM cyclosporin A) are shown in the bottom. The results are representatives of 3 experiments.

(data not shown). The transmembrane potential of mitochondria energized with succinate was assessed in the presence of Ca^{2+} by using a cationic dye, rhodamine 123 as an indicator. Incubation of mitochondria with NAPQI (50 μM) caused a decrease in membrane potential in the presence of Ca^{2+} and the mitochondrial depolarization was also prevented by the addition of cyclosporin A (Fig. 6 insert).

4. Discussion

The present study demonstrates that in vivo treatment of male CD-1 mice with acetaminophen results in MPT and suggests that the MPT is involved in pathogenesis of acetaminophen-induced liver injury. Although a number of mitochondrial proteins have been identified as targets of covalent binding of NAPQI, a reactive metabolite of acetaminophen [8,9], the pathogenic role of the covalent binding in the toxicity has not been fully elucidated. On the other hand, MPT was recently proposed as a mechanism of the acetaminophen hepatotoxicity associated with the covalent binding [21,22]. Indeed, the other reports presented protective effect of cyclosporin A against the acetaminophen toxicity [35,36]. However, one of them observed the protective effect of combination of cyclosporin A, fructose and trifluoperazine against acetaminophen hepatotoxicity [35], and thus the contribution of blocking MPT to the overall protection remains unknown. Another assessed the systemic toxicity (LD_{50}) but not liver injury as in vivo toxicity of acetaminophen [36]. Therefore, the present data indicating that cyclosporin A protected mice against acetaminophen-induced liver injury is the first report to demonstrate the in vivo pathogenic role of MPT in the hepatotoxicity of acetaminophen.

Several mechanisms may underlie acetaminophen-induced, probably NAPQI-mediated MPT. MPT pore constitutes a complex assembly of voltage-dependent anion channel in the outer membrane, adenine nucleotide translocase in the inner membrane and cyclophilin D in the matrix [34]. None of these proteins has reported to be a direct target of the covalent binding of NAPQI, allowing us to postulate the oxidative damage of the mitochondrial membrane protein(s) by NAPQI, because it possesses oxidant characteristics [37]. Indeed, it has been reported that mitochondrial NADPH and protein thiols were oxidized by NAPQI [38]. If the membrane thiol is oxidized, essentially thiol cross-linkage is formed, the conformation is changed, followed by opening of the pore. Adenine translocator has been proposed as a protein to form cross-linkage [39]. It was reported that late treatment of acetaminophen-treated mouse hepatocytes with dithiothreitol, a thiol-reducing agent, but not *N*-acetylcysteine prevented the liver injury [40], suggesting that reversal of an oxidation state, which increases the probability of the open state of the pore, is effective for the hepatoprotection.

On the other hand, the voltage-dependent regulation of the MPT pore has been characterized by depolarization of the membrane ant resultant increase in probability of the pore opening. An important factor determining the voltage gating potential of the MPT pore is also redox state of vicinal cysteine thiols, which are closely associated with the voltage-sensing element of the MPT pore [41]. These findings suggest the mitochondrial oxidative stress is responsible for occurrence of MPT. Furthermore, it was reported that NAPQI was able to raise cell calcium probably by inhibition of plasma membrane Ca^{2+}-ATPase through its depleting effect on GSH and protein-bound SH groups [10]. The increase in cellular Ca^{2+} in vivo should sensitize liver mitochondria to NAPQI-induced MPT pore opening.

Various changes caused by MPT and associated with toxicity are presented, which include membrane depolarization, uncoupling of oxidative phosphorylation, and release intramitochondrial ions and metabolic intermediates [10]. Among them, MPT as a source of superoxide was proposed to be an important event in acetaminophen hepatotoxicity [21,22]. The generation of superoxide supports the theory that oxidative stress in addition to covalent binding is involved in the acetaminophen hepatotoxicity. In the present study, acetaminophen-induced mitochondrial oxidative stress was suppressed by cyclosporin A (Fig. 3). It is thus suggested that the mitochondrial oxidative damage is the result of MPT, as well as the cause of MPT as described above. Furthermore, depletion of mitochondrial ATP in the acetaminophen-treated mice was also attenuated by cyclosporin A (Fig. 3), which occurs as a result of the MPT [34]. Recent studies have suggested that nitric oxide (NO) as well as superoxide is involved in the acetaminophen-induced liver injury [42,43]. NO is known to trap superoxide and generate peroxynitrite, which is highly reactive and toxic. Because peroxynitrite also induces MPT [44], the MPT may provide the mechanism how NO participates in the acetaminophen hepatotoxicity, although we have not investigated NO-dependent pathways in the present study.

We detected leakage of cytochrome c into cytosol in the acetaminophen-treated mice, which is correlated with MPT pore opening (Fig. 4). The leakage were slightly attenuated by cyclosporin A, supporting our conclusion that the protection against acetaminophen hepatotoxicity is accounted for by the protection against MPT. Furthermore, leakage of cytochrome c implies induction of apoptosis because cytochrome c is known to be a signal of apoptosis cascade by activating caspases such as caspase 9 and then caspase 3 [45]. Acetaminophen could induce hepatocyte apoptosis in vitro as well as necrosis, whereas the quantitative determination of cell death after exposure of hepatotoxic dose of acetaminophen in vivo indicated that acetaminophen caused extensively oncotic necrosis rather than apoptosis [20]. Thus, it is reasonable to postulate that necrotic cell death is mainly induced also in the present study, although we have not determined the type of cell death. It is considered that depletion of ATP induced by the MPT and by other events prevents the apoptotic cell death, which requires ATP [46], in acetaminophen-induced liver injury. On the other hand, it was recently reported that although caspases and apoptosis were important in initiating the acetaminophen-induced liver injury, the apoptotic pathway was only incompletely activated in response to acetaminophen treatment, and instead it degenerated to induce premature secondary necrosis [47].

In conclusion, MPT can explain the mechanism for acetaminophen-induced liver injury in vivo in mice, which is based on the consensus that mitochondria are the important target in the acetaminophen hepatotoxicity. NAPQI is considered to play an important role in the MPT. Suppression of the MPT resulted in protection not only from acetaminophen-induced liver injury but also from the known events closely related to the pathogenesis in the hepatotoxicity. Because the MPT is down-stream of covalent binding of NAPQI to the hepatocellular targets and linked with the secondary oxidative stress, it is suggested that blocking MPT should be a strategy for development of therapeutic agent for the acetaminophen overdose, which can be administrated later than *N*-acetylcysteine, which contributes to detoxify NAPQI.

Acknowledgements

This study was supported in part by a grant-in-aid from the Ministry of Education, Science and Culture of Japan.

References

[1] Mitchell JR, Jollow DJ, Potter WZ, Davis DC, Gillette JR, Brodie BB. Acetaminophen-induced hepatic necrosis. I. Role of drug metabolism. J Pharmacol Exp Ther 1973;187:185–194.

[2] Dahlin DC, Miwa GT, Lu AY, Nelson SD. *N*-Acetyl-*p*-benzoquinone imine: a cytochrome P-450-mediated oxidation product of acetaminophen. Proc Natl Acad Sci USA 1984;81:1327–1331.

[3] Jollow DJ, Mitchell JR, Potter WZ, Davis DC, Gillette JR, Brodie BB. Acetaminophen-induced hepatic necrosis. II. Role of covalent binding in vivo. J Pharmacol Exp Ther 1973;187:195–202.

[4] Mitchell JR, Jollow DJ, Potter WZ, Gillette JR, Brodie BB. Acetaminophen-induced hepatic necrosis. IV. Protective role of glutathione. J Pharmacol Exp Ther 1973;187:211–217.

[5] Manautou JE, Emeigh Hart SG, Khairallah EA, Cohen SD. Protection against acetaminophen hepatotoxicity by a single dose of clofibrate: effects on selective protein arylation and glutathione depletion. Fundam Appl Toxicol 1996;29:229–237.

[6] Tarloff JB, Khairallah EA, Cohen SD, Goldstein RS. Sex- and age-dependent acetaminophen hepato- and nephrotoxicity in Sprague-Dawley rats: role of tissue accumulation, nonprotein sulfhydryl depletion, and covalent binding. Fundam Appl Toxicol 1996;30:13–22.

[7] Schnellmann JG, Pumford NR, Kusewitt DF, Bucci TJ, Hinson JA. Deferoxamine delays the development of the hepatotoxicity of acetaminophen in mice. Toxicol Lett 1999;106:79–88.

[8] Cohen SD, Pumford NR, Khairallah EA, Boekelheide K, Pohl LR, Amouzadeh HR, et al. Selective protein covalent binding and target organ toxicity. Toxicol Appl Pharmacol 1997;143:1–12.

[9] Qiu Y, Benet LZ, Burlingame AL. Identification of the hepatic protein targets of reactive metabolites of acetaminophen in vivo in mice using two-dimensional gel electrophoresis and mass spectrometry. J Biol Chem 1998;273:17940–17953.
[10] Moore M, Thor H, Moore G, Nelson S, Moldeus P, Orrenius S. The toxicity of acetaminophen and *N*-acetyl-*p*-benzoquinone imine in isolated hepatocytes is associated with thiol depletion and increased cytosolic Ca^{2+}. J Biol Chem 1985;260:13035–13040.
[11] Burcham PC, Harman AW. Acetaminophen toxicity results in site-specific mitochondrial damage in isolated mouse hepatocytes. J Biol Chem 1991;266:5049–5054.
[12] Harman AW, Kyle ME, Serroni A, Farber JL. The killing of cultured hepatocytes by *N*-acetyl-*p*-benzoquinone imine (NAPQI) as a model of the cytotoxicity of acetaminophen. Biochem Pharmacol 1991;41: 1111–1117.
[13] Nazareth WM, Sethi JK, McLean AE. Effect of paracetamol on mitochondrial membrane function in rat liver slices. Biochem Pharmacol 1991;42:931–936.
[14] Parmar DV, Ahmed G, Khandkar MA, Katyare SS. Mitochondrial ATPase: a target for paracetamol-induced hepatotoxicity. Eur J Pharmacol 1995;293:225–229.
[15] Gupta S, Rogers LK, Taylor SK, Smith CV. Inhibition of carbamyl phosphate synthetase-I and glutamine synthetase by hepatotoxic doses of acetaminophen in mice. Toxicol Appl Pharmacol 1997;146: 317–327.
[16] Bernardi P. The permeability transition pore control points of a cyclosporin A-sensitive mitochondrial channel involved in cell death. Biochim Biophys Acta 1996;1275:5–9.
[17] Lemasters JJ, Nieminen AL, Qian T, Trost LC, Elmore SP, Nishimura Y, et al. The mitochondrial permeability transition in cell death: a common mechanism in necrosis, apoptosis and autophagy. Biochim Biophys Acta 1998;1366:177–196.
[18] Masubuchi Y, Nakayama S, Horie T. Role of mitochondrial permeability transition in diclofenac-induced hepatocyte injury in rats. Hepatology 2002;35:544–551.
[19] Zoratti M, Szabo I. The mitochondrial permeability transition. Biochim Biophys Acta 1995;1241:139–176.
[20] Gujral JS, Knight TR, Farhood A, Bajt ML, Jaeschke H. Mode of cell death after acetaminophen overdose in mice: apoptosis or oncotic necrosis? Toxicol Sci 2002;67:322–328.
[21] Jaeschke H, Knight TR, Bajt ML. The role of oxidant stress and reactive nitrogen species in acetaminophen hepatotoxicity. Toxicol Lett 2003;144:279–288.
[22] James LP, McCullough SS, Lamps LW, Hinson JA. Effect of *N*-acetylcysteine on acetaminophen toxicity in mice: relationship to reactive nitrogen and cytokine formation. Toxicol Sci 2003;75: 458–467.
[23] Schneider WC, Hogeboom GH. Intracellular distribution of enzymes. V. Further studies on the distribution of cytochrome c in liver homogenate. J Biol Chem 1950;183:123–128.
[24] Lowry OH, Rosebrough NJ, Farr AL, Randall RJ. Protein measurement with the folin phenol reagent. J Biol Chem 1951;193:265–275.
[25] Keller DA, Menzel DB. Picomole analysis of glutathione, glutathione disulfide, glutathione S-sulfonate, and cysteine S-sulfonate by high-performance liquid chromatography. Anal Biochem 1985;151: 418–423.
[26] Emaus RK, Grunwald R, Lemasters JJ. Rhodamine 123 as a probe of transmembrane potential in isolated rat-liver mitochondria: spectral and metabolic properties. Biochim Biophys Acta 1986;850:436–448.
[27] Berg-Candolfi M, Candolfi E, Benet LZ. Suppression of intestinal and hepatic cytochrome P4503A in murine toxoplasma infection Effects of *N*-acetylcysteine and *N*(G)-monomethyl-L-arginine on the hepatic suppression. Xenobiotica 1996;26:381–394.
[28] Lee SS, Buters JT, Pineau T, Fernandez-Salguero P, Gonzalez FJ. Role of CYP2E1 in the hepatotoxicity of acetaminophen. J Biol Chem 1996;271:12063–12067.
[29] Sinclair JF, Szakacs JG, Wood SG, Walton HS, Bement JL, Gonzalez FJ, et al. Short-term treatment with alcohols causes hepatic steatosis and enhances acetaminophen hepatotoxicity in Cyp2e1(−/−) mice. Toxicol Appl Pharmacol 2000;168:114–122.
[30] Zhang J, Huang W, Chua SS, Wei P, Moore DD. Modulation of acetaminophen-induced hepatotoxicity by the xenobiotic receptor CAR. Science 2002;298:422–424.
[31] Wolf A, Trendelenburg CF, Diez-Fernandez C, Prieto P, Houy S, Trommer WE, et al. Cyclosporine A-induced oxidative stress in rat hepatocytes. J Pharmacol Exp Ther 1997;280:1328–1334.
[32] Knight TR, Kurtz A, Bajt ML, Hinson JA, Jaeschke H. Vascular and hepatocellular peroxynitrite formation during acetaminophen toxicity: role of mitochondrial oxidant stress. Toxicol Sci 2001;62:212–220.
[33] Jaeschke H. Glutathione disulfide formation and oxidant stress during acetaminophen-induced hepatotoxicity in mice in vivo: the protective effect of allopurinol. J Pharmacol Exp Ther 1990;255:935–941.
[34] Kim JS, He L, Lemasters JJ. Mitochondrial permeability transition: a common pathway to necrosis and apoptosis. Biochem Biophys Res Commun 2003;304:463–470.
[35] Beales D, McLean AE. Protection in the late stages of paracetamol-induced liver cell injury with fructose, cyslosporin A and trifluoperazine. Toxicology 1996;107:201–208.
[36] Haouzi D, Cohen I, Vieira HL, Poncet D, Boya P, Castedo M, et al. Mitochondrial permeability transition as a novel principle of hepatorenal toxicity in vivo. Apoptosis 2002;7:395–405.
[37] Powis G, Svingen BA, Dahlin DC, Nelson SD. Enzymatic and non-enzymatic reduction of *N*-acetyl-*p*-benzoquinone imine and some properties of the *N*-acetyl-*p*-benzosemiquinone imine radical. Biochem Pharmacol 1984;33:2367–2370.
[38] Weis M, Moore GA, Cotgreave IA, Nelson SD, Moldeus P. Quinone imine-induced Ca^{2+} release from isolated rat liver mitochondria. Chem Biol Interact 1990;76:227–240.
[39] Brustovetsky N, Klingenberg M. Mitochondrial ADP/ATP carrier can be reversibly converted into a large channel by Ca^{2+}. Biochemistry 1996;35:8483–8488.
[40] Grewal KK, Racz WJ. Intracellular calcium disruption as a secondary event in acetaminophen-induced hepatotoxicity. Can J Physiol Pharmacol 1993;71:26–33.
[41] Petronilli V, Costantini P, Scorrano L, Colonna R, Passamonti S, Bernardi P. The voltage sensor of the mitochondrial permeability transition pore is tuned by the oxidation-reduction state of vicinal thiols. Increase of the gating potential by oxidants and its reversal by reducing agents. J Biol Chem 1994;269:16638–16642.
[42] Bourdi M, Masubuchi Y, Reilly TP, Amouzadeh HR, Martin JL, George JW, et al. Protection against acetaminophen-induced liver injury and lethality by interleukin 10: role of inducible nitric oxide synthase. Hepatology 2002;35:289–298.
[43] Gardner CR, Laskin JD, Dambach DM, Sacco M, Durham SK, Bruno MK, et al. Reduced hepatotoxicity of acetaminophen in mice lacking inducible nitric oxide synthase: potential role of tumor necrosis factor-alpha and interleukin-10. Toxicol Appl Pharmacol 2002;184:27–36.
[44] Radi R, Cassina A, Hodara R, Quijano C, Castro L. Peroxynitrite reactions and formation in mitochondria. Free Radic Biol Med 2002; 33:1451–1464.
[45] Cai J, Yang J, Jones DP. Mitochondrial control of apoptosis: the role of cytochrome c. Biochim Biophys Acta 1998;1366:139–149.
[46] Eguchi Y, Shimizu S, Tsujimoto Y. Intracellular ATP levels determine cell death fate by apoptosis or necrosis. Cancer Res 1997;57:1835–1840.
[47] El-Hassan H, Anwar K, Macanas-Pirard P, Crabtree M, Chow SC, Johnson VL, et al. Involvement of mitochondria in acetaminophen-induced apoptosis and hepatic injury: roles of cytochrome c, Bax, Bid, and caspases. Toxicol Appl Pharmacol 2003;191:118–129.

JOURNAL OF VIROLOGY, Jan. 2005, p. 1271–1281 Vol. 79, No. 2
0022-538X/05/$08.00+0 doi:10.1128/JVI.79.2.1271–1281.2005

Molecular Determinants for Subcellular Localization of Hepatitis C Virus Core Protein

Ryosuke Suzuki,[1] Shinichiro Sakamoto,[1] Takeya Tsutsumi,[1] Akiko Rikimaru,[1,2] Keiko Tanaka,[3] Takashi Shimoike,[1] Kohji Moriishi,[4] Takuya Iwasaki,[3,5] Kiyohisa Mizumoto,[2] Yoshiharu Matsuura,[4] Tatsuo Miyamura,[1] and Tetsuro Suzuki[1]*

Department of Virology II, National Institute of Infectious Diseases, Shinjuku-ku,[1] Department of Biochemistry, School of Pharmaceutical Sciences, Kitasato University, Minato-ku,[2] and Department of Pathology, National Institute of Infectious Diseases, Shinjuku-ku,[3] Tokyo, Research Center for Emerging Infectious Diseases, Research Institute for Microbial Diseases, Osaka University, Suita-shi, Osaka,[4] and Department of Pathology, Institute of Tropical Medicine, Nagasaki University, Nagasaki-shi, Nagasaki,[5] Japan

Received 21 June 2004/Accepted 26 July 2004

Hepatitis C virus (HCV) core protein is a putative nucleocapsid protein with a number of regulatory functions. In tissue culture cells, HCV core protein is mainly located at the endoplasmic reticulum as well as mitochondria and lipid droplets within the cytoplasm. However, it is also detected in the nucleus in some cells. To elucidate the mechanisms by which cellular trafficking of the protein is controlled, we performed subcellular fractionation experiments and used confocal microscopy to examine the distribution of heterologously expressed fusion proteins involving various deletions and point mutations of the HCV core combined with green fluorescent proteins. We demonstrated that a region spanning amino acids 112 to 152 can mediate association of the core protein not only with the ER but also with the mitochondrial outer membrane. This region contains an 18-amino-acid motif which is predicted to form an amphipathic α-helix structure. With regard to the nuclear targeting of the core protein, we identified a novel bipartite nuclear localization signal, which requires two out of three basic-residue clusters for efficient nuclear translocation, possibly by occupying binding sites on importin-α. Differences in the cellular trafficking of HCV core protein, achieved and maintained by multiple targeting functions as mentioned above, may in part regulate the diverse range of biological roles of the core protein.

Hepatitis C virus (HCV), the most important causative agent of posttransfusion and sporadic non-A, non-B hepatitis, is a positive-stranded RNA virus belonging to the family *Flaviviridae* (7). A precursor polyprotein of about 3,000 amino acids is encoded by a large open reading frame of the genome and undergoes cellular and viral protease-mediated posttranslational modification to produce a series of structural and nonstructural proteins (8, 13, 16).

HCV core protein, which is derived from the N terminus of the viral polyprotein, forms multimers and interacts physically with the viral RNA to constitute the nucleocapsid (28, 47, 50). Tissue transglutaminase is responsible for stabilizing the core protein by cross-linking it into a dimeric form (26). In addition, the core viral protein has properties which enable it to modulate a number of cellular processes, including transcription, inhibition or stimulation of apoptosis, and suppression of host immunity, as reviewed previously (21, 29, 51, 52). Several studies suggest that expression of the core protein affects mitochondrial function and lipid metabolism. The core protein increases the cellular production of reactive oxygen species with subsequent increases in lipid peroxidation (35, 39). The viral protein also colocalizes with human apolipoprotein AII, associates with lipid droplets, and has the capacity to influence metabolic events involving lipid storage (2, 17, 30, 36, 44). In addition, the core protein reduces microsomal triglyceride transfer, leading to defects in very low density lipoprotein assembly and secretion (40). Furthermore, the HCV core protein has transforming potential in some cells under certain conditions (5, 42). Transgenic mice expressing this protein in the liver develop hepatic steatosis due to increased oxidative stress in the absence of inflammation, with subsequent development of hepatocellular carcinoma (34, 36). These results suggest that the HCV core protein might play a pivotal role in the pathogenesis of hepatitis C in addition to its role as a structural component of the viral capsid.

The amino acid sequence of the core protein is well conserved among different HCV isolates and genotypes compared to other HCV proteins. The N-terminal domain of the HCV core protein is highly basic, while its C terminus is hydrophobic. Although several core proteins of various sizes exist (17 to 23 kDa) (15, 23, 25, 49, 56), two processing events result in the predominant production of a 21-kDa core protein. Both of these events utilize the endoplasmic reticulum (ER). The first one is to be cleaved from downstream envelope protein E1 at position 191, where the C-terminal hydrophobic domain serves as a putative signal peptide sequence. Subsequently, the signal sequence of 13 or 18 residues is processed by signal peptide peptidase (19, 23, 56).

The HCV core protein is found primarily within the membranes of cytoplasmic organelles, but it is also found in the nucleus (23, 48, 56). Immunofluorescence studies show a punc-

* Corresponding author. Mailing address: Department of Virology II, National Institute of Infectious Diseases, 1-23-1 Toyama, Shinjuku-ku, Tokyo, Japan 162-8640. Phone: (81) 3-5285-1111. Fax: (81) 3-5285-1161. E-mail: tesuzuki@nih.go.jp.

tate pattern, consistent with ER localization, as well as perinuclear localization (15, 24, 32, 46, 56). Some studies suggest direct effects of the core protein on mitochondrial function. In fact, the core protein localizes to the mitochondria (34, 39). The N-terminal domain of the core protein contains three stretches of arginine- and lysine-rich sequences. Translocation of the core protein to the nucleus, mediated by these basic-residue stretches which function as nuclear localization signals (NLSs), is observed (6, 48). In addition, Moriishi et al. demonstrated that the N-terminal region of the core protein is also essential for nuclear retention through its interaction with the proteasome activator PA28γ (33).

In this study, we found a region that is important for localization of the mature core protein to the ER and to the mitochondrial outer membrane. We also identified a novel bipartite NLS responsible for nuclear targeting of the core protein, presumably via an importin-dependent pathway.

MATERIALS AND METHODS

Plasmid construction. The construction of a plasmid expressing the full-length core protein of 191 amino acids, pCAGC191, was described previously (49). pGFP, a construct expressing green fluorescent protein (GFP) with a C-terminal Myc epitope tag sequences, was prepared as follows. pCMV/Myc/mito/GFP (Invitrogen Corp., Carlsbad, Calif.) was digested with PmlI, followed by treatment with the Klenow fragment of DNA polymerase I. The resultant linear fragment was ligated to a PstI linker (GCTGCAGC) and digested with PstI to remove the mitochondrial targeting signal sequence, followed by self-ligation. A series of HCV core-GFP fusion constructs were made by amplifying the core gene fragments with PCR with primers containing Flag epitope tag sequences (sense) and a PstI site (both). After digestion with PstI, the segments were inserted into the PstI site of pGFP. A series of GFP-core-E1 fusion constructs were made by amplifying core and E1 gene fragments with PCR with primers containing a NotI site. After digestion with NotI, the segments were inserted into the NotI site of pGFP.

pGEX-4T-1 (Amersham Bioscience Corp., Piscataway, N.J.) was used to express core protein fused with glutathione *S*-transferase (GST) in *Escherichia coli*. Core cDNA fragments encoding amino acids 1 to 71 were inserted into the EcoRI site of pGEX-4T-1. Alanine substitutions were introduced into the core protein by PCR mutagenesis with primers containing base alterations. The PCR products were then cloned into pCR2.1 (Invitrogen Corp.) and verified by DNA sequencing. Individual cDNAs were excised and inserted separately into pGFP or pGEX-4T-1. The primer sequences used in this study are available from the authors upon request.

Plasmid pRSET-hSRP1α (54), containing importin-α cDNA under the control of a T7 promoter, was kindly provided by Karsten Weis (University of California, Berkeley). A cDNA clone of importin-α possessing 14 residues (MYPYDVP DYGGGGS), derived in part from the hemagglutinin (HA) tag at the N terminus, was constructed by PCR. The resultant linear fragment was inserted under the control of a CAG promoter of pCAGGS and designated pCAG-HA-imp.

Cell culture and transfection. Human embryonic kidney 293T cells were maintained in Dulbecco's modified Eagle's medium supplemented with 100 units of penicillin per ml, 100 μg of streptomycin per ml, and 10% fetal bovine serum at 37°C in a 5% CO_2 incubator. Monolayers of 293T cells were transfected with plasmid DNA in the presence of Lipofectamine (Gibco-BRL, Life Technologies, Gaithersburg, Md.) according to the manufacturer's instructions.

Confocal immunofluorescence microscopy. Transfected cells were grown on glass coverslips. Two days after transfection, cells were fixed with 4% paraformaldehyde in phosphate-buffered saline (PBS) for 20 min at room temperature. Intracellular localization of HCV core-GFP fusion proteins was visualized in cells transfected with a variety of GFP fusion constructs.

In order to detect the HCV core protein by immunofluorescence, fixed cells were permeabilized with 0.2% Triton X-100 in PBS for 3 min at room temperature, followed by blocking with a nonfat milk solution (Block Ace; Snow Brand Milk Products Co., Sapporo, Japan). The cells were then incubated with anticore monoclonal antibody B2 (Anogen, Mississauga, Canada) for 60 min at room temperature, followed by incubation with fluorescein isothiocyanate-conjugated rabbit anti-mouse immunoglobulin G (IgG) (ICN Pharmaceuticals, Aurora, Ohio) for 45 min. To visualize mitochondria, MitoTracker Red CM-H_2XRos (Molecular Probes, Eugene, Oreg.) was added to the culture medium to a final concentration of 100 nM and incubated for 120 min at 37°C prior to fixation. To visualize the ER, goat anticalregulin antibody (Santa Cruz Biotechnology, Santa Cruz, Calif.) and rhodamine-conjugated rabbit anti-goat IgG (ICN Pharmaceuticals) were used as the first and second antibodies, respectively. To visualize HA-importin-α, mouse anti-HA antibody (Roche Molecular Biochemicals, Indianapolis, Ind.) and rhodamine-conjugated goat anti-mouse IgG (ICN Pharmaceuticals) were used as the first and second antibodies, respectively. All specimens were examined with an LSM510 laser scanning confocal microscope (Carl Zeiss, Oberkochen, Germany).

Immunoelectron microscopy. Cells were transfected as described above. After 2 days, cells were fixed with 3% paraformaldehyde and 0.1% glutaraldehyde in 0.1 M PBS (pH 7.4). Free aldehyde groups were quenched with 50 mM NH_4Cl in PBS. The cell pellets were embedded at progressively lower temperatures (down to −35°C) in Lowicryl k4M according to an established protocol (43). Ultrathin sections were prepared and mounted on carbon-coated nickel grids. To perform electron microscopy, Lowicryl k4M ultrathin sections, mounted on grids, were floated on a droplet of PBS containing 1% bovine serum albumin, 0.1% Triton X-100, and 0.1% Tween 20 for 10 min, after which they were exposed to droplets of mouse anticore monoclonal antibody (Anogen) diluted in PBS for 45 min. Following this, they were rinsed twice for 5 min each in PBS and incubated with anti-mouse IgG-coated 10-nm immunogold particles (British Biocell, Cardiff, United Kingdom) for 45 min. After rinsing with PBS and distilled water, the grids and embedded sections were air dried and exposed to uranyl and lead acetate contrast agents.

Subcellular fractionation. All steps were performed at 4°C in the presence of a protease inhibitor cocktail called Complete (Roche Molecular Biochemicals). To isolate the ER fraction, transfected cells were washed with PBS, lysed in homogenization buffer A (50 mM Tris-HCl [pH 8.0], 1 mM β-mercaptoethanol, 1 mM EDTA, and 0.32 M sucrose), and then centrifuged at 5,000 × *g* for 10 min. The supernatant was then collected and centrifuged at 105,000 × *g* for 1 h. The pellet was disrupted in lysis buffer (50 mM Tris-HCl [pH 7.5], 150 mM NaCl, 1% NP-40, 1 mM dithiothreitol, 1 mM sodium orthovanadate, and 10 mM sodium fluoride), after which it was centrifuged at 15,000 × *g* for 20 min. The resulting supernatant was used as the ER fraction.

To isolate the mitochondrial fraction, transfected cells were washed with PBS and homogenized in ice-cold homogenization buffer B (200 mM mannitol, 50 mM sucrose, 1 mM EDTA, and 10 mM Tris-HCl) at pH 7.4. The supernatant was then centrifuged at 1,000 × *g* for 10 min to remove large debris and nuclei. The resulting supernatant was then centrifuged at 20,000 × *g* for 20 min to obtain crude mitochondria. The crude mitochondria pellet was subfractionated in Nycodenz gradients for further purification of mitochondria. Nycodenz (Axis-Shield PoC AS, Oslo, Norway) solution at 50% (wt/vol) was prepared in buffer containing 5 mM Tris-HCl and 1 mM EDTA at pH 7.4. This stock solution was then diluted with buffer containing 0.25 M sucrose, 5 mM Tris-HCl, and 1 mM EDTA at pH 7.4 before use. The crude mitochondrial pellets was suspended in 4 ml of 25% Nycodenz solution and overlaid onto the following discontinuous Nycodenz gradients: 1 ml of 40%, 1 ml of 34%, and 2 ml of 30%. The samples were topped off with 2 ml of 23% Nycodenz solution after placement onto the discontinuous gradients. The tubes were then centrifuged at 52,000 × *g* for 90 min. The dense band seen after centrifugation at the 25 to 30% interface was recovered as the purified mitochondrial fraction.

To determine the submitochondrial localization pattern of the core protein, mitochondria were resuspended in SH buffer (0.6 M sorbitol and 20 mM HEPES-KOH [pH 7.2]) in the absence or presence of 30 μg of proteinase K per ml after purification by Nycodenz density gradient centrifugation. Samples were incubated for 30 min at 0°C, after which protease digestion was halted by the addition of *p*-aminophenyl methanesulfonyl fluoride hydrochloride (*p*-APMSF) (5 mM). Proteins lysed in sodium dodecyl sulfate (SDS) sample buffer were analyzed by SDS-polyacrylamide gel electrophoresis (PAGE) and immunoblotted as described below.

Immunoblot analysis. The proteins were transferred to a polyvinylidene difluoride membrane (Immobilon; Millipore, Tokyo, Japan) after separation by SDS-PAGE. After blocking, the membranes were probed with monoclonal- or polyclonal-antibody against core protein (Anogen), prohibitin (Neo Markers, Fremont, Calif.), ribophorin I (Santa Cruz Biotechnology), translocase of the outer membrane (Tom) 20 (Santa Cruz Biotechnology), translocase of the inner membrane (Tim) 17 (Santa Cruz Biotechnology), or GFP (Santa Cruz Biotechnology). Immunoblots were developed as previously described (15).

GST pulldown assay. *Escherichia coli* BL21 cells were transformed with GST-core fusion plasmids and grown at 37°C. Expression of the fusion protein was induced by 1 mM isopropyl-β-D-thiogalactopyranoside at 37°C for 3 h. Bacteria were harvested, suspended in lysis buffer (1% Triton X-100 in PBS), and soni-

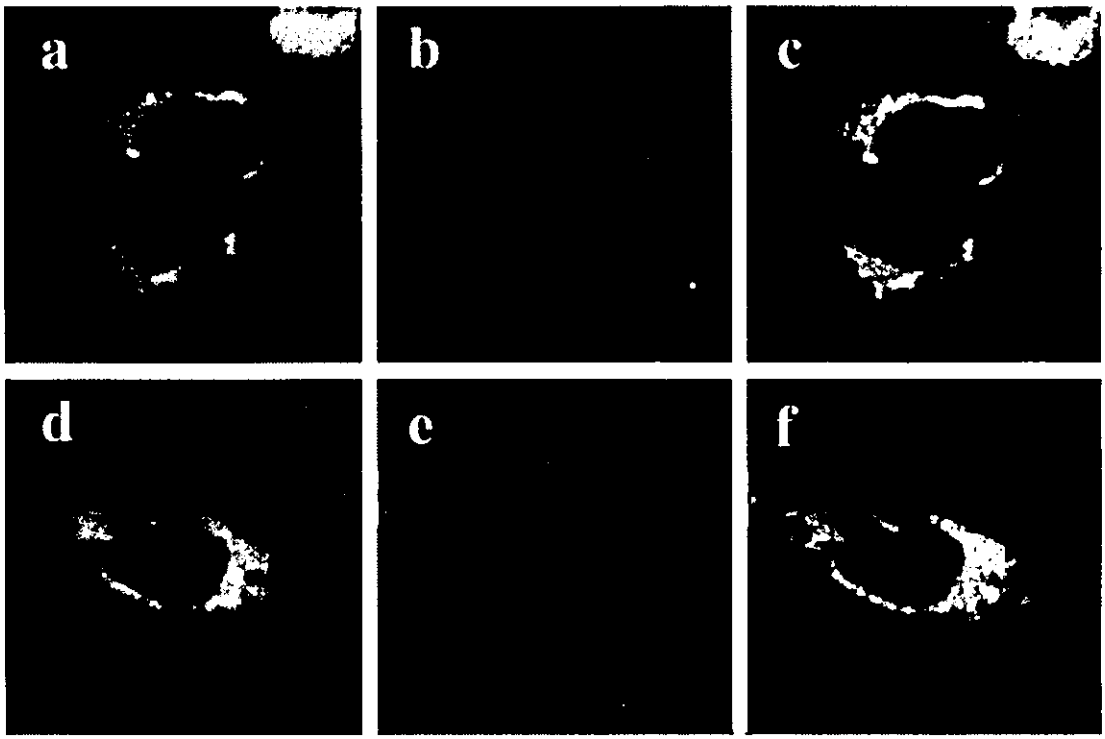

FIG. 1. Confocal analysis of double staining for HCV core protein and ER or mitochondria. 293T cells transfected with full-length HCV core expression plasmid, pCAGC191 were allowed to express the plasmid for 2 days. Transfected cells were fixed directly (a to c) or fixed after loading with Mitotracker (d to f). After permeabilization with Triton X-100, cells were subjected to immunofluorescence staining with a mouse anticore antibody. A goat anticalregulin antibody was used for ER staining. The green signals corresponding to the core were found with a fluorescein isothiocyanate-conjugated rabbit anti-mouse IgG (a and d). The red signals corresponding to the ER were obtained with a rhodamine-conjugated rabbit anti-goat IgG secondary antibody (b). Mitochondria were stained with the mitochondrion-selective dye Mitotracker (e). Overlay resulted in yellow signals indicative of colocalization (c and f).

cated on ice. GST and GST fusion proteins were purified from bacterial lysates with glutathione-Sepharose beads (Amersham Bioscience Corp.). The beads were washed four times with lysis buffer. Approximately equal amounts of purified protein, as estimated by Coomassie brilliant blue staining, were used for the binding assays. For pulldown assays, in vitro transcription and translation of importin-α was done with pRSET-hSRP1α and the TNT-coupled reticulocyte lysate system (Promega Corp., Madison, Wis.) with T7 RNA polymerase. The reaction was carried out at 30°C for 4 h in the presence of [^{35}S]methionine/cysteine (ICN Pharmaceuticals). The translation product was then incubated with glutathione-Sepharose beads bound to GST fusion proteins in 1 ml of binding buffer (40 mM HEPES [pH 7.5], 100 mM KCl, 0.1% NP-40, and 20 mM 2-mercaptoethanol) at 4°C for 1 h. The beads were washed four times with binding buffer, and the pulldown complexes were separated by SDS-PAGE on 15% polyacrylamide gels. The gels were then fixed, dried, and analyzed with autoradiography.

RESULTS

Subcellular localization of HCV core protein. To assess the subcellular localization of HCV core protein, we first analyzed cells transfected with a full-length core-expressing construct by confocal microscopy. In accordance with previous observations (2, 15, 32, 45, 56), a granular cytoplasmic staining pattern of the core protein was observed in 293T (Fig. 1) and human hepatoblastoma HepG2 (data not shown) cells. Dual staining of transfected cells with antibody against the ER protein calregulin along with anticore antibody confirmed the ER localization of the core protein (Fig. 1a, b, and c show the core,

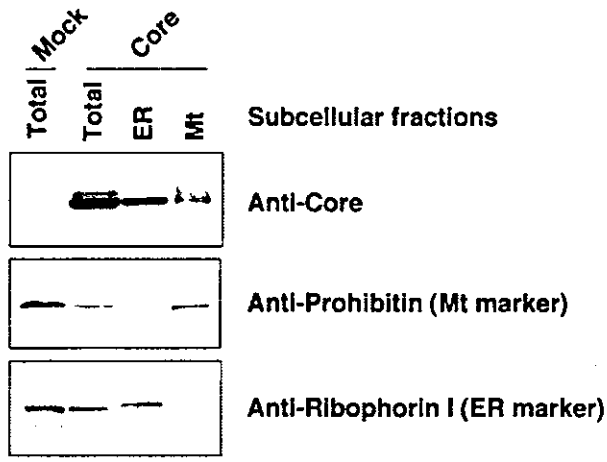

FIG. 2. Subcellular distribution of HCV core protein analyzed by immunoblotting. ER and mitochondrial (Mt) fractions were isolated from 293T cells expressing the full-length core protein (Core) or nontransfected cells (Mock) 2 days after transfection. Equal amounts of protein from each fraction as well as whole cell lysates (Total) were subjected to immunoblotting with a monoclonal antibody against either HCV core, prohibitin, or ribophorin I.

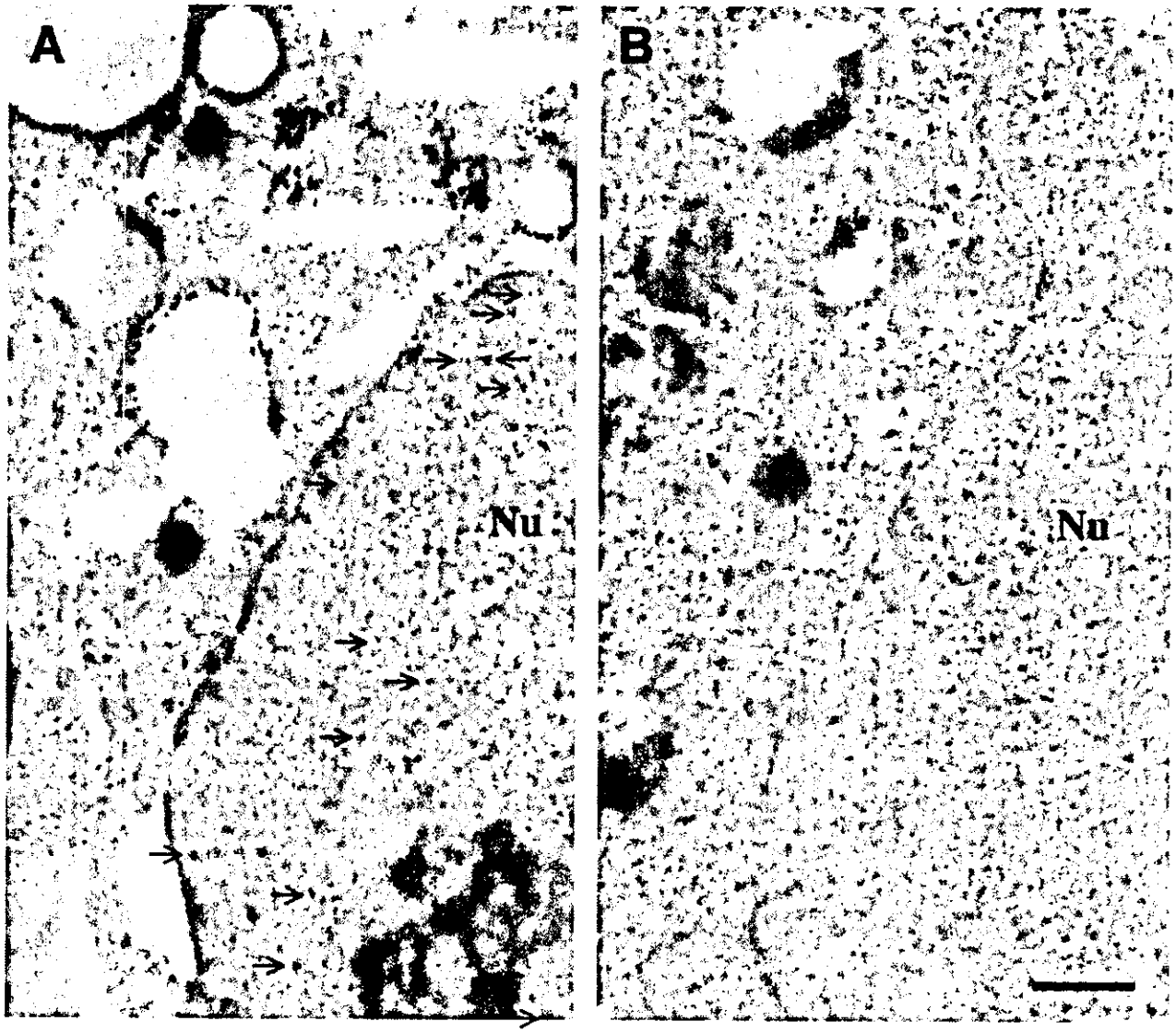

FIG. 3. Immunoelectron microscopy of HCV core protein. 293T cells expressing the full-length core protein (A) and nonexpressing cells (B) fixed 2 days after transfection. Immunoelectron microscopic analysis was performed with a mouse anticore antibody and a secondary anti-mouse IgG conjugated with gold particles. The arrows indicate the core protein localized in the nucleus (Nu). Bar, 500 nm.

calregulin, and a merged image, respectively). The pattern of subcellular localization of the core protein (Fig. 1d) was compared to the distribution of mitochondria, as revealed by MitoTracker staining (Fig. 1e). Although distribution of the core protein was not completely identical with that of the mitochondrion-selective dye, overlapping staining was observed, particularly in the perinuclear region (Fig. 1f).

Intracellular localization of the core protein was further examined in 293T cells by subcellular fractionation and Western blotting. The core protein was present in both the ER and mitochondrial fractions (Fig. 2), while it was not detected in the cytosol fraction (data not shown). The purity of the ER and mitochondrial fractions was confirmed with antibodies against ribophorin I as an ER marker and prohibitin as a mitochondrial marker.

It is generally difficult to identify the nuclear distribution of proteins of interest due to contamination of the nuclear preparation with unbroken, intact cells. Thus, to investigate whether the core protein localizes to the nucleus, we examined transfected cells by immunoelectron microscopy. Although gold particles were primarily observed within cytoplasmic membranes, perhaps highlighting the ER, immunoreactivity to anticore antibody was also observed in the nucleus (Fig. 3A, arrows). In contrast, no antibody labeling was observed in cells transfected with an empty vector (Fig. 3B).

Thus, HCV core protein predominates in the cytoplasm in a membrane-associated form(s) with ER and mitochondria, but nuclear localization is also observed.

Regions responsible for directing core protein to the ER and mitochondria. Given the tendency of the core protein to lo-

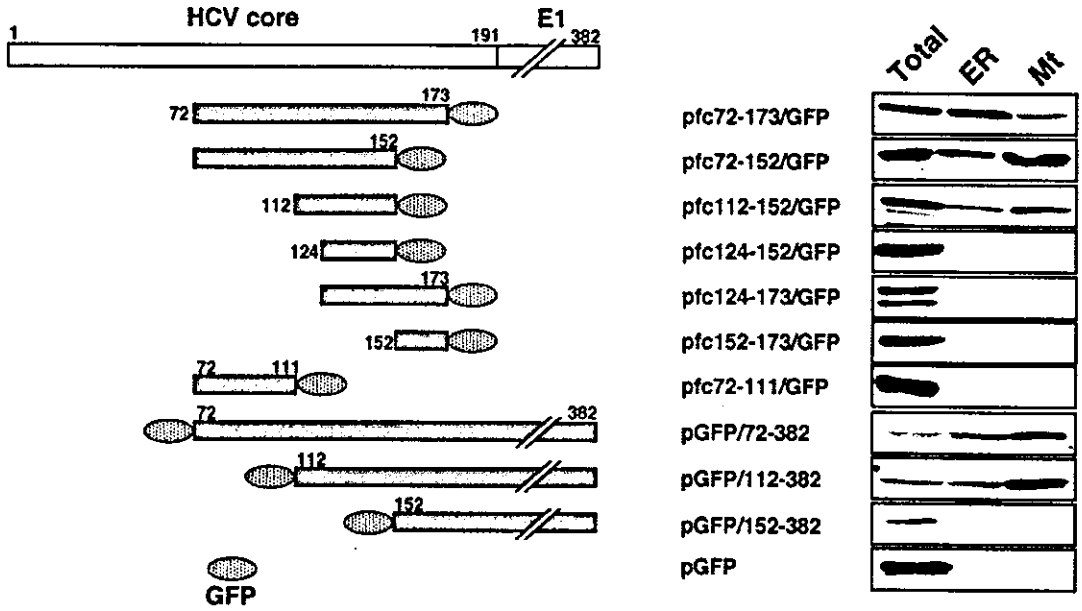

FIG. 4. Identification of segments that mediate association with ER and mitochondria in the core protein. Schematic diagram (left) and nomenclature (middle) of the core-GFP fusions are shown. Gray bars, expressed core and E1 regions. Subcellular distribution of fusion proteins is indicated on the right. ER and mitochondrial (Mt) fractions as well as whole-cell lysates (Total) were subjected to immunoblotting with an anti-GFP antibody.

calize to the ER and to mitochondria, we next investigated whether specific sequences might be responsible for transporting the core protein to these organelles. Fusion proteins between different regions of the core protein and GFP were developed, with specific emphasis on the region downstream of amino acid 72 because this region contains clusters of hydrophobic amino acids and the N-terminal 71 residues of the core are known to play a role in nuclear targeting (6, 48).

Western blotting of subcellular fractions with anti-GFP antibody revealed the localization of a core (72–173)-GFP fusion protein to the ER and to mitochondria (Fig. 4). Fusion proteins containing GFP and core proteins with N- or C-terminal deletions (72-152-GFP and 112-152-GFP) were likewise identified within the ER and mitochondrial fractions. In contrast, the ER and mitochondrial fractions did not contain GFP fusion proteins containing core protein amino acids 124 to 152, 124 to 173, 152 to 173, or 72 to 111. These fusion proteins demonstrated distribution profiles similar to that of GFP alone. We also tested GFP-core-E1 fusions, which are processed at the C terminus of the core by signal peptidase and signal peptide peptidase (19, 30). GFP-core fusions expressed from pGFP/72–382 and pGFP/112–382 were detected in the ER and mitochondrial fractions. The fusion expressed from pGFP/152–382 was not identified in these fractions.

We further analyzed subcellular localization of the fusion proteins by confocal immunofluorescence microscopy (Fig. 5). As expected, fusions of (72–173)-GFP and (112–152)-GFP exhibited localization to the ER and mitochondria. The patterns of subcellular localization of these fusions are indistinguishable from that of the full-length core protein, as shown in Fig. 1. Expression of (124–152)-GFP or (112–123)-GFP resulted in widespread diffusion of the fusion in the cell. Thus, these results indicate that the region spanning amino acids 112 to 152 can mediate association of the core protein not only to the ER but also to the mitochondria.

We subsequently examined the submitochondrial localization of the core protein with a protease protection assay. As shown in Fig. 6A, HCV core protein localized in the mitochondria was completely digested upon treatment with proteinase K for 30 min at 0°C. Under identical conditions, a marker specific for the mitochondrial outer membrane, Tom20, was also observed to disappear, whereas digestion of a mitochondrial inner membrane marker, Tim17, was not observed. These findings confirm that HCV core protein is localized to the mitochondrial outer membrane.

The predicted secondary structure of the region, amino acids 72 to 173, is shown in Fig. 6B. The presence of a long helical segment, lying between amino acids 116 and 134, and two short α-helices (amino acids 146 to 152 and amino acids 155 to 159) were predicted. The results of the cell fractionation assay and confocal microscopy with a series of deletion mutants shown in Fig. 4 and 5 suggest that an α-helix between amino acids 116 and 134 may be required for associating the core protein with the ER and the mitochondrial outer membrane. When amino acids 117 to 134 are portrayed as a helical wheel, we found an amphipathic structure with hydrophobic residues on one side and polar residues on the other side of the α-helix (Fig. 6C), which is often observed in membrane-associated proteins. This helical conformation might be important for directing the core protein to the ER and mitochondrial outer membranes.

Nuclear localization of the HCV core protein is mediated by a bipartite NLS, possibly via an importin-dependent pathway. Although HCV core protein is mainly localized within the cytoplasm, it is also found in the nucleus, as shown in Fig. 3.

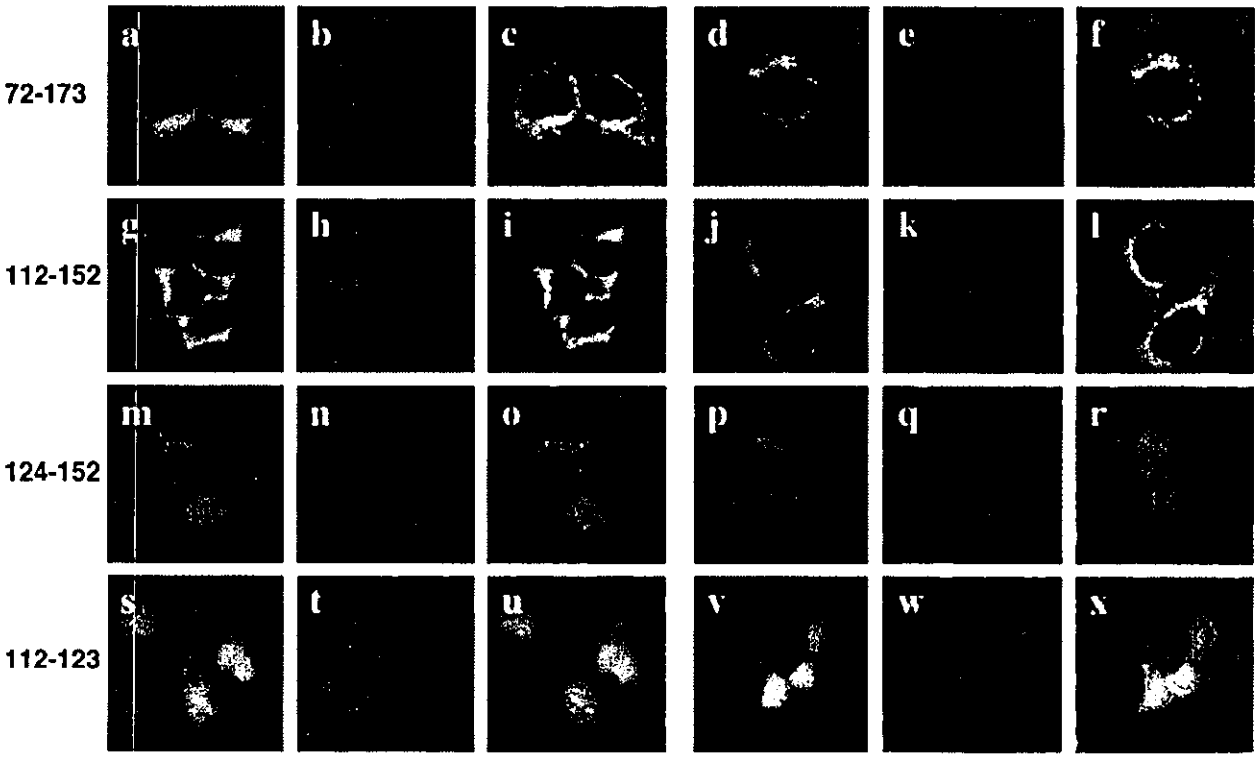

FIG. 5. Confocal analysis of double staining for core-GFP fusion protein and ER or mitochondria. 293T cells transfected with core-GFP expression plasmids (72–173, 112–152, 124–152, and 112–123) were allowed to express the plasmid for 2 days. Transfected cells were fixed directly (a to c, g to i, m to o, and s to u) or fixed after loading with Mitotracker (d to f, j to l, p to r, and v to x). After permeabilization with Triton X-100, a goat anticalregulin antibody was used for ER staining. The red signals corresponding to the ER were obtained with a rhodamine-conjugated rabbit anti-goat IgG secondary antibody (b, h, n, and t). Mitochondria were stained with the mitochondrion-selective dye Mitotracker (e, k, q, and w). Overlay resulted in yellow signals indicative of colocalization (c, f, i, l, o, r, u, and x).

The results of previous studies demonstrate that the N-terminal region of the core protein is responsible for nuclear targeting. It contains three clusters of basic amino acid residues that represent putative consensus motifs for NLS sequences PKPQRKTKR (amino acids 5 to 13), PRRGPR (amino acids 38 to 43), and PRGRRQPIPKARRP (amino acids 58 to 71) (6, 48). Nuclear targeting is generally governed by a family of transporters or cytosolic receptor proteins, known as importins or karyopherins, which function in concert with a guanine nucleotide-binding protein named Ran and other regulatory proteins such as NTF2/p10. Conventional NLS-dependent nuclear targeting occurs when importin-α recognizes the NLS sequence, mediating binding to importin-β1, after which the trimeric complex translocates to the nucleus (12).

In order to determine whether the putative NLS motifs identified within the core protein sequence are capable of binding to importin-α, we examined the in vitro interaction between bacterially expressed GST-fused core protein and ^{35}S-labeled importin-α with a GST pulldown assay. We then substituted lysine and arginine residues of one or more of the putative NLS motifs of the core protein (all contained within the first 71 amino acids of the N terminus) with alanine and fused the resultant constructs with GST, as shown schematically in Fig. 7A. As shown in Fig. 7B (upper panel), importin-α was pulled down by a GST fusion protein containing wild-type core (amino acids 1 to 71) protein but not with GST alone, suggesting that direct binding occurs between the core protein and importin-α. Importin-α was also pulled down by GST-core fusion proteins containing substitutions in one or two NLS motifs (NLS/m1, NLS/m2, NLS/m3, NLS/m4, NLS/m5, and NLS/m6). However, importin-α was not pulled down by GST-core fusion proteins containing alanine substitutions in all three NLS motifs (NLS/m7). It should be noted that similar amounts of GST fusion proteins were used for each of the in vitro pulldown assays, followed by SDS-PAGE and Coomassie brilliant blue staining (Fig. 7B, lower panel). These results demonstrated that all three putative NLS motifs of the N-terminal region of the core protein can mediate binding to importin-α, which suggests that nuclear translocation of the core protein occurs via an importin-dependent pathway (12).

The interaction between the core and importin-α was further analyzed by a colocalization assay (Fig. 7C). The GFP fusion containing the wild-type core (amino acids 1 to 71) was well colocalized with HA-importin-α; distribution of the two proteins showed similar nuclear staining patterns, confirming the presence of a functional NLS sequence(s) within the core protein. In contrast, NLS/m4, with substitutions in two NLS motifs, was partly colocalized with HA-importin-α near or around the nuclear membrane, suggesting that NLS motif double mutants bind to importin-α but their binding efficiency is lower than that of wild-type core protein.

Finally, we examined the subcellular localization of core

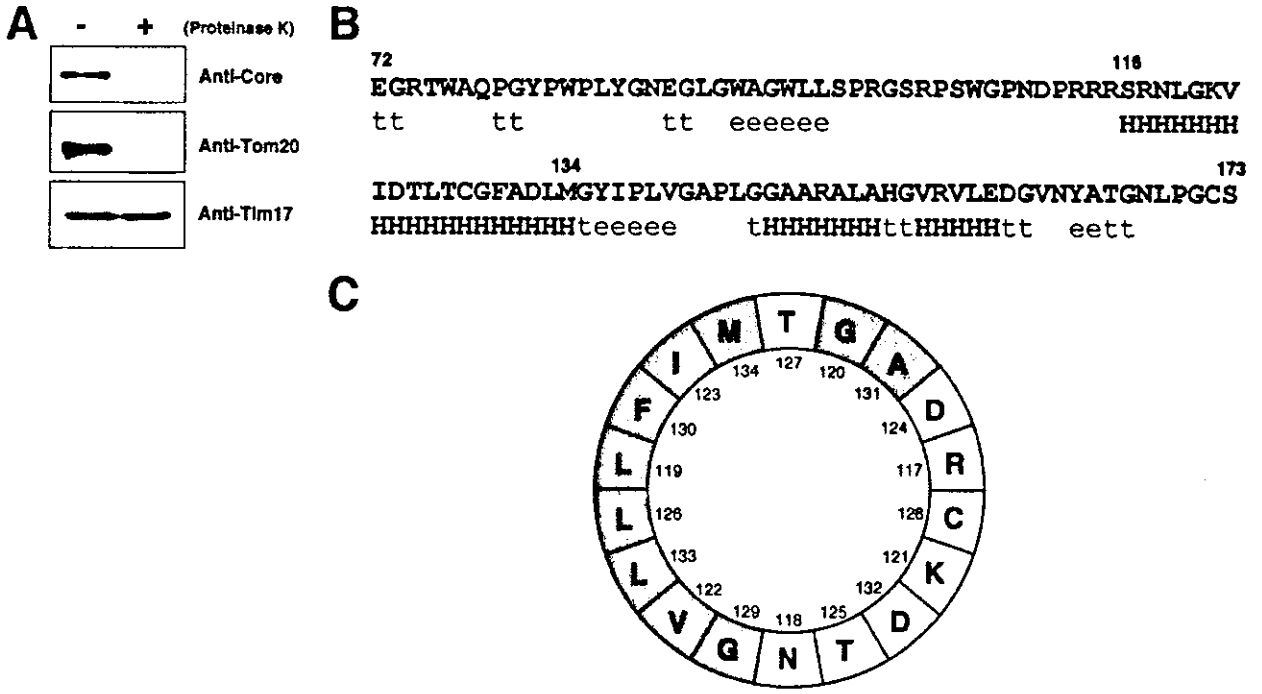

FIG. 6. (A) Protease protection assay. A mitochondrial fraction isolated from cells expressing the core protein was treated with proteinase K (+) as described in Materials and methods. The sample as well as the nontreated fraction (−) were subjected to immunoblotting with a monoclonal antibody against either HCV core, Tom20, or Tim17. (B) Protein sequence and predicted secondary structure of HCV core, amino acids 72 to 173. The secondary structure prediction was obtained with the self-optimized prediction method, a computer program on the internet (http://npsa-pbil.ibcp.fr/cgi-bin/npsa_automat.pl?page = /NPSA/npsa_sopm.html). H, α-helix; t, turn; e, extension. (C) α-Helical plot of amino acids 117 to 134 of the core protein. In the helical wheel plots, the gray shading represents apolar and hydrophobic residues; and the white represents polar residues.

protein expressed by the wild-type and NLS mutants (Fig. 7D). As expected, a fusion protein containing wild-type core protein (amino acids 1 to 71) and GFP was localized exclusively to the nucleus. Core proteins from three fusion proteins containing substitutions in each NLS motif (NLS/m1, NLS/m2, and NLS/m3) were detected primarily in the nucleus. Weak fluorescence was also observed in the cytoplasm, suggesting that these mutations caused a slight reduction in the efficiency of nuclear translocation. On the other hand, two or three NLS motif substitution mutations (NLS/m4, NLS/m5, NLS/m6, and NLS/m7) completely abolished nuclear translocation, resulting in a diffuse distribution of core protein, similar to that of GFP alone. Although it is likely that all three putative NLS motifs play a role, the above results suggest that at least two of the three putative NLS motifs are prerequisite for efficient nuclear translocation of the core protein.

DISCUSSION

HCV core protein is released from the viral polyprotein by a host protease(s) within the ER membrane at a signal peptide sequence lying between the core and envelope (E1) proteins (16, 41). Subsequently, the signal peptide is further processed by an intramembranous protease called signal peptide peptidase (38, 53). This mature form of the core protein is then released and undergoes subcellular trafficking (30, 53). The core protein localizes mainly to the ER, mitochondria, and lipid droplets. Some reports also describe localization of the core protein to the nuclei of hepatocytes in HCV-infected patients (10), transgenic mice (34), and cultured cells expressing viral polyproteins (56). Although it has been reported which sequence motifs are responsible for localization of the HCV core protein to lipid droplets and nuclei, it is uncertain which sequences target the core protein to the ER and to mitochondria. In this study, we identified sequences related to localization of the mature core protein to the ER and to mitochondria.

Through heterologous expression of core-GFP fusion proteins containing a series of deletions, we determined that a sequence extending from amino acids 112 to 152 of the core protein is required for its localization at the mitochondrial outer membrane. Translocation of nucleus-encoded mitochondrial proteins is usually dependent on N-terminal sequences, referred to as mitochondrial targeting sequences (37). However, it is also true that a significant proportion of mitochondrial proteins lack these N-terminal mitochondrial targeting sequences. Specifically, a number of outer membrane proteins do not have cleavable sequences at their N termini; rather, they are targeted to mitochondria by means of internal or C-terminal signals (31).

Since it has been reported that amino acid sequences required for targeting to the outer mitochondrial membrane form a highly hydrophobic α-helical wheel, as seen in A-kinase associated protein 84/12 (4) and NADH-cytochrome *b* reduc-

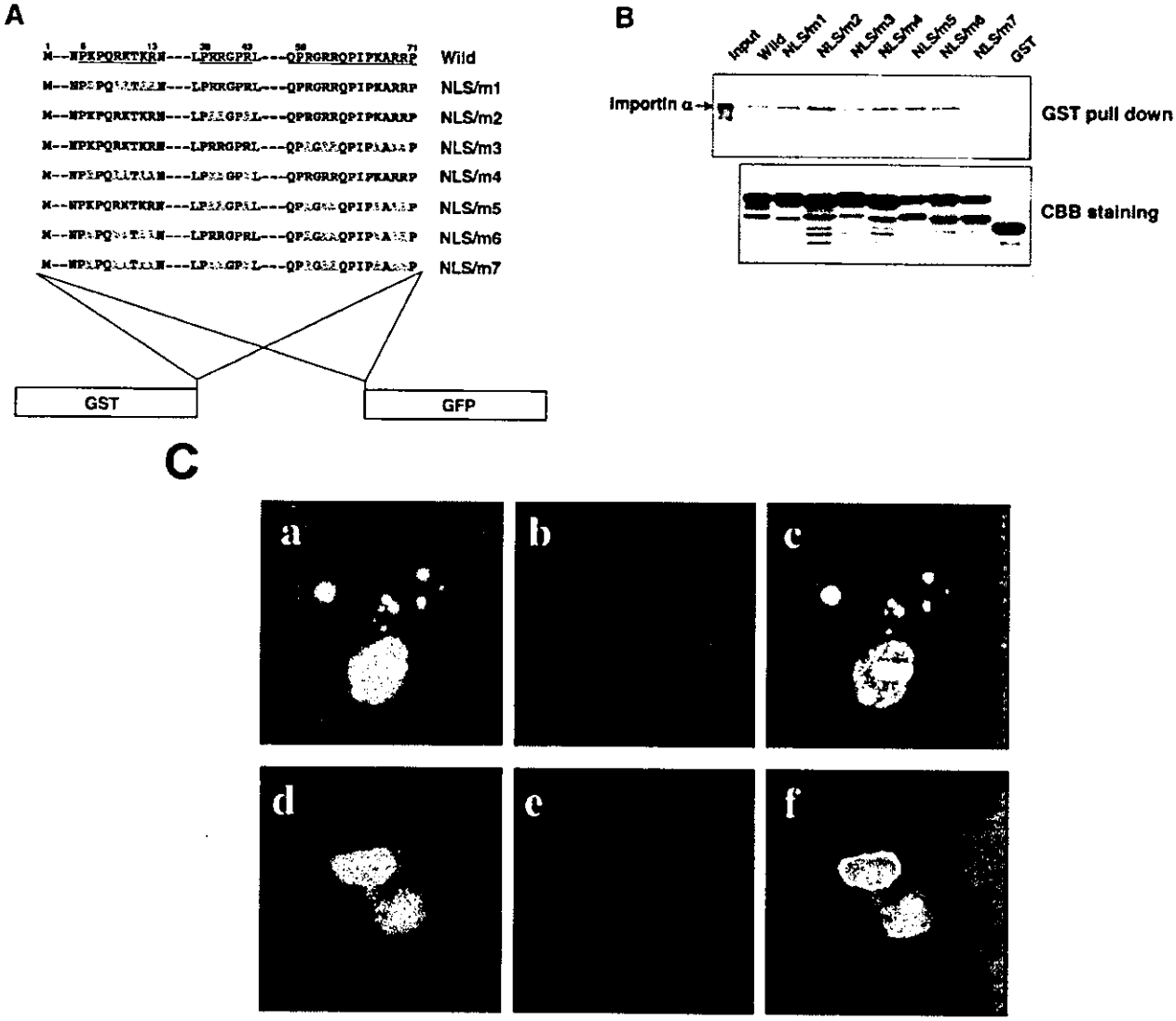

FIG. 7. Mutational analyses of NLS motifs in HCV core protein. (A) Schematic structures of fusion proteins and amino acid sequences corresponding to putative NLS motifs, three basic clusters (underlined) in the core protein. Two series of constructs fused with either GFP or GST were created. The mutated basic residues are indicated with outline letters. (B) GST pulldown assay. Equal amounts of GST fusions as described in A or GST alone was immobilized on glutathione-Sepharose 4B beads and incubated with in vitro-translated, [^{35}S]methionine-labeled importin-α. Bound material was separated by SDS-PAGE, and the amount of importin-α bound was detected by autoradiography. Direct electrophoretic separation of in vitro translation products served as a control (input). Coomassie brilliant blue staining of GST fusions and GST alone are shown in the bottom panel. (C) Confocal analysis of double staining for core-GFP fusion protein and HA-importin-α. 293T cells transfected with the wild-type core (1–71)-GFP (a to c) or NLS/m4 (d to f) expression plasmid and pCAG-HA-imp were allowed to express for 2 days. After the cells were fixed and permeabilized, they were incubated with a mouse anti-HA antibody. The red signals corresponding to HA-importin-α were obtained with a rhodamine-conjugated goat anti-mouse IgG secondary antibody (b and e). Overlay resulted in yellow signals indicative of colocalization (c and f). (D) Subcellular localization of GFP fusion proteins. GFP fusions with and without substitution mutations in the NLS motifs of the core protein as described in A were expressed in 293T cells. GFP images of the fixed cells were recorded.

tase (14), a predicted structure of an amphipathic α-helix present between amino acids 116 and 134 (Fig. 6B and C) possibly plays a role in directing the core protein to the mitochondrial outer membrane. Sequence comparisons demonstrate conservation of the amino acid sequence and secondary structure of the region, amino acids 112 to 152, among a variety of HCV isolates, including the infectious H77c clone (55), as well as a full-length adaptive replicon (3). To gain insight into the significance of the secondary structure of the region in targeting to the mitochondria, further structural and biochemical analyses are needed.

The association of HCV core protein with the mitochondrial membrane suggests that the core protein has the ability to modulate mitochondrial function, possibly by altering the permeability of the mitochondrial membrane. The core protein induces the production of cellular reactive oxygen species in

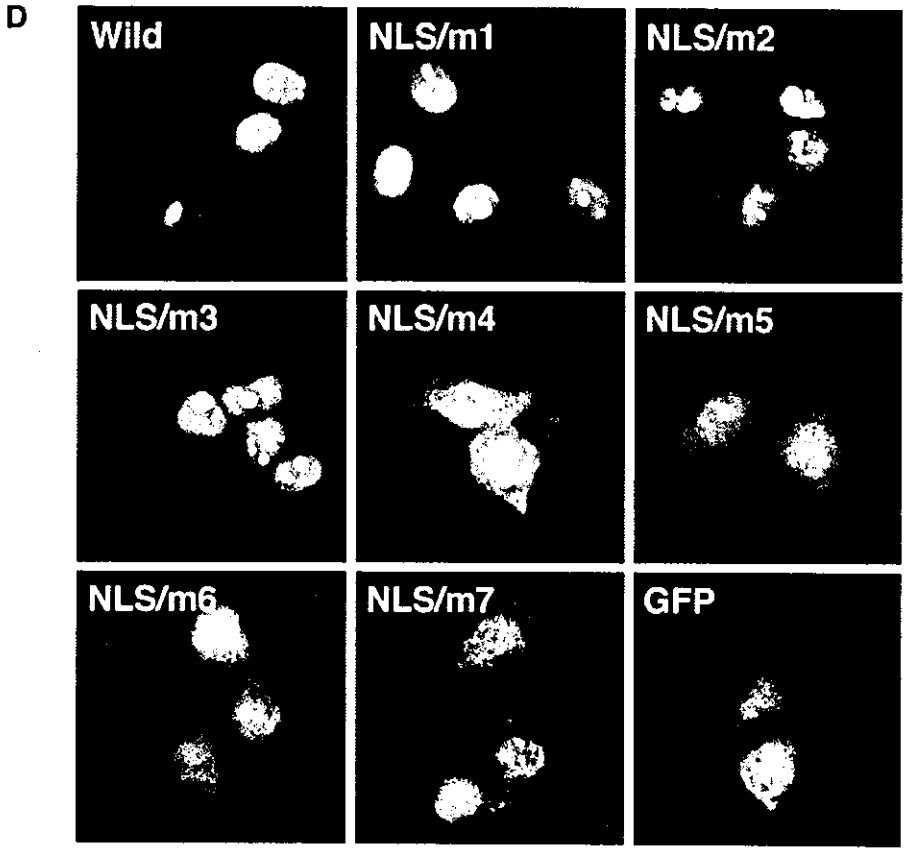

FIG. 7—*Continued.*

the livers of core-transgenic mice and in core-expressing cell lines (35). Reactive oxygen species, predominantly generated in mitochondria, induce genetic mutations and act as secondary messengers to regulate a variety of cellular functions, including gene expression and proliferation (1). Although the molecular mechanism by which core protein induces reactive oxygen species production is still unclear, HCV core protein is known to impair the mitochondrial electron transfer system (35). The core protein may also modulate apoptosis, since mitochondria play a major role in regulating programmed cell death. Expression of HCV proteins, including the core protein, suppresses the release of cytochrome *c* from mitochondria to the cytoplasm in HCV-transgenic mice, thus inhibiting Fas-mediated apoptosis (27).

Okamoto et al. recently reported that not only the C-terminal signal sequence but also amino acids 128 to 151 are required for ER retention of the core protein by using a series of N-terminally truncated core protein constructs (38). Here, in this study, we further showed that amino acids 112 to 152 mediate association of the core protein with the ER in the absence of the C-terminal signal sequence. Hope and McLauchlan demonstrated that the central domain of the core protein, amino acids 119 to 174, is important for association with lipid droplets (17). They also showed that this corresponding domain is shared with GB virus B, which is most closely related to HCV, but not with either pestiviruses or flaviviruses (18). It appears that the 41 residues identified as the sequence mediating association with the ER membrane in the present study are crucial for directing the core protein to lipid droplets, since the surface of lipid droplets must derive from the cytoplasmic side of the ER membrane.

The HCV core protein contains NLS sequences which are composed of three stretches of sequences rich in basic residues. These sequences were originally identified by experiments with fused forms of wild-type and mutated core proteins with β-galactosidase (6, 48). C-terminally truncated versions of the core protein localize exclusively to the nucleus (48). A fraction of the core protein is detected in the nucleus even when full-length HCV core gene is expressed (Fig. 2) and as described (34, 56). However, it is difficult to demonstrate clearly the nuclear localization of the core protein by immunofluorescence, presumably because of the instability of nuclearly localized core protein (49, 33). We only observed a nuclear staining pattern of the matured core protein after adding proteasome inhibitors to the culture (33).

Generally, NLS sequences fall into two categories; (i) monopartite NLSs, which contain a single cluster of basic residues, and (ii) bipartite NLSs, which contain two clusters of basic residues separated by an unconserved linker sequence of variable length (reviewed in reference 12). Nuclear translocation of an NLS-containing cargo protein is initiated when the soluble import receptor (importin) recognizes the NLS-contain-

ing protein within the cytoplasm. Importin-α contains an NLS-binding site(s), and importin-β docks importin-cargo complexes to the cytoplasmic filaments of a nuclear pore complex, after which translocation occurs through the nuclear pore. Thus, importin-α functions as an adaptor between the bona fide import receptor and the NLS-containing protein.

We further characterized the NLS of the core protein and found that each of the NLS motifs of the core protein is able to bind to importin-α and that at least two NLS motifs are required for efficient nuclear distribution of the core protein in cells. It appears that double mutations among three NLS motifs decrease the ability of the core protein to bind importin-α. These observations suggest that the binding of the double mutants with importin-α leads to no or little active translocation of the core protein into the nucleus. The double mutations may also block subsequent interactions with importin-β1, GTPase Ran, and/or NTF2/p10, which are required for translocation through the nuclear pore complexes.

The findings obtained in this study suggest that HCV core protein NLS motifs have a bipartite function. Crystallographic studies of monopartite (e.g., simian virus 40 large T antigen) and bipartite (e.g., nucleoplasmin) NLSs show that the basic residue clusters of bipartite NLSs occupy separate binding sites on importin-α. In contrast, while monopartite NLSs can bind to the same sites as bipartate NLSs on importin-α, they mainly bind to the N-terminal binding site, which is referred to as the major binding site on importin-α (9, 11). A recent report describes an importin-α variant with a mutation in the major site which results in decreased ability to bind both monopartite and bipartite NLSs. Another variant with a mutation in the minor site exhibits decreased binding only to bipartite NLS-containing proteins, making importin-α nonfunctional in vivo (22). Thus, we favor a model in which the core protein bipartite NLS, composed of any two of the three basic clusters, occupies both major and minor binding sites on importin-α, resulting in efficient nuclear translocation. Importin-α may be equally accessible to all clusters, given their close proximity to one another, as well as the distinct conformational flexibility of the ≈70-residue N-terminal region of the core protein.

With regard to the molecular mechanisms participating in nuclear localization of the core protein, Moriishi et al. found that PA28γ is involved in nuclear localization of the core protein. Interaction of the core protein with PA28γ plays an important role in retention of the core protein in the nucleus (33). Furthermore, in yeast cells, nuclear transport of the core protein requires the activity of the small GTPase Ran/Gsp1p and is mediated by Kap123p, but neither importin-α nor importin-β is involved (20). Differences in nucleocytoplasmic transport between yeast and mammalian cells might explain the inconsistencies observed in the present study. Further experiments are required to characterize the exact nature of the interaction between the core protein and components of the nuclear import machinery, particularly in cells where HCV is replicating.

In conclusion, the mature HCV core protein has an internal 41-amino-acid sequence mediating association of the viral protein with the ER and mitochondria. We also provide evidence for a novel class of bipartite NLS contained within the core protein, which comprises two of three basic motifs, thus enabling efficient nuclear targeting. Multiple functional domains influence the subcellular localization of the core protein, which ultimately depends on the balance of the respective signals.

ACKNOWLEDGMENTS

We thank colleagues in the laboratories of the Department of Virology II at the National Institute of Infectious Diseases of Japan for providing advice and help. We especially thank Mami Matsuda and Makiko Yahata for assistance in sequencing and the preparation of experimental reagents and Tomoko Mizoguchi for secretarial work. We are grateful to Karsten Weis for providing us with the plasmid containing importin-α cDNA.

This work was supported in part by Second Term Comprehensive 10-Year Strategy for Cancer Control and Research on Emerging and Reemerging Infectious Diseases, Health Sciences Research Grants of the Ministry of Health, Labor and Welfare, and by the Program for Promotion of Fundamental Studies in Health Sciences of the Organization for Drug ADR Relief, R&D Promotion and Product Review of Japan (ID:01–3). This work was also supported in part by a Grant-in-Aid for Young Scientists from the Ministry of Education, Culture, Sports, Science and Technology to R.S. (15790244).

REFERENCES

1. **Adler, V., Z. Yin, K. D. Tew, and Z. Ronai.** 1999. Role of redox potential and reactive oxygen species in stress signaling. Oncogene **18**:6104–6111.
2. **Barba, G., F. Harper, T. Harada, M. Kohara, S. Goulinet, Y. Matsuura, G. Eder, Z. Schaff, M. J. Chapman, T. Miyamura, and C. Bréchot.** 1997. Hepatitis C virus core protein shows a cytoplasmic localization and associates to cellular lipid storage droplets. Proc. Natl. Acad. Sci. USA **94**:1200–1205.
3. **Bukh, J., T. Pietschmann, V. Lohmann, N. Krieger, K. Faulk, R. E. Engle, S. Govindarajan, M. Shapiro, M. St Claire, and R. Bartenschlager.** 2002. Mutations that permit efficient replication of hepatitis C virus RNA in Huh-7 cells prevent productive replication in chimpanzees. Proc. Natl. Acad. Sci. USA **99**:14416–14421.
4. **Cardone, L., T. de Cristofaro, A. Affaitati, C. Garbi, M. D. Ginsberg, M. Saviano, S. Varrone, C. S. Rubin, M. E. Gottesman, E. V. Avvedimento, and A. Feliciello.** 2002. A-kinase anchor protein 84/121 are targeted to mitochondria and mitotic spindles by overlapping amino-terminal motifs. J. Mol. Biol. **320**:663–675.
5. **Chang, J., S. H. Yang, Y. G. Cho, S. B. Hwang, Y. S. Hahn, and Y. C. Sung.** 1998. Hepatitis C virus core from two different genotypes has an oncogenic potential but is not sufficient for transforming primary rat embryo fibroblasts in cooperation with the H-ras oncogene. J. Virol. **72**:3060–3065.
6. **Chang, S. C., J. H. Yen, H. Y. Kang, M. H. Jang, and M. F. Chang.** 1994. Nuclear localization signals in the core protein of hepatitis C virus. Biochem. Biophys. Res. Commun. **205**:1284–1290.
7. **Choo, Q. L., G. Kuo, A. J. Weiner, L. R. Overby, D. W. Bradley, and M. Houghton.** 1989. Isolation of a cDNA clone derived from a blood-borne non-A, non-B viral hepatitis genome. Science **244**:359–362.
8. **Choo, Q. L., K. H. Richman, J. H. Han, K. Berger, C. Lee, C. Dong, C. Gallegos, D. Coit, R. Medina-Selby, P. J. Barr, et al.** 1991. Genetic organization and diversity of the hepatitis C virus. Proc. Natl. Acad. Sci. USA **88**:2451–2455.
9. **Conti, E., M. Uy, L. Leighton, G. Blobel, and J. Kuriyan.** 1998. Crystallographic analysis of the recognition of a nuclear localization signal by the nuclear import factor karyopherin alpha. Cell **94**:193–204.
10. **Falcon, V., N. Acosta-Rivero, G. Chinea, M. C. de la Rosa, I. Menendez, S. Duenas-Carrera, B. Gra, A. Rodriguez, V. Tsutsumi, M. Shibayama, J. Luna-Munoz, M. M. Miranda-Sanchez, J. Morales-Grillo, and J. Kouri.** 2003. Nuclear localization of nucleocapsid-like particles and HCV core protein in hepatocytes of a chronically HCV-infected patient. Biochem. Biophys. Res. Commun. **310**:54–58.
11. **Fontes, M. R., T. Teh, and B. Kobe.** 2000. Structural basis of recognition of monopartite and bipartite nuclear localization sequences by mammalian importin-alpha. J. Mol. Biol. **297**:1183–1194.
12. **Görlich, D., and U. Kutay.** 1999. Transport between the cell nucleus and the cytoplasm. Annu. Rev. Cell. Dev. Biol. **15**:607–660.
13. **Grakoui, A., D. W. McCourt, C. Wychowski, S. M. Feinstone, and C. M. Rice.** 1993. Characterization of the hepatitis C virus-encoded serine proteinase: determination of proteinase-dependent polyprotein cleavage sites. J. Virol. **67**:2832–2843.
14. **Hahne, K., V. Haucke, L. Ramage, and G. Schatz.** 1994. Incomplete arrest in the outer membrane sorts NADH-cytochrome b5 reductase to two different submitochondrial compartments. Cell **79**:829–839.
15. **Harada, S., Y. Watanabe, K. Takeuchi, T. Suzuki, T. Katayama, Y. Takebe, I. Saito, and T. Miyamura.** 1991. Expression of processed core protein of hepatitis C virus in mammalian cells. J. Virol. **65**:3015–3021.
16. **Hijikata, M., N. Kato, Y. Ootsuyama, M. Nakagawa, and K. Shimotohno.** 1991. Gene mapping of the putative structural region of the hepatitis C virus